4. THE TROPICS—H. J. Diamond, Ed.

a. Overview—H. J. Diamond

The year was characterized by a transition from waning La Niña conditions to a building El Niño, which developed in June and then strengthened to what NOAA's Climate Prediction Center (CPC) considers to be a strong episode. By December, SSTs were more than 2.0°C above average over large parts of the central and eastern equatorial Pacific from 175°W to 90°W.

Overall global tropical cyclone (TC) activity during 2009 was the lowest since 2006, with six of the seven main hurricane basins (the exception is the Eastern North Pacific) experiencing near-normal or somewhat below normal TC activity. The El Niño contributed to what is only the second below-normal hurricane season for the Atlantic basin since 1995 and at the same time contributed to a sharp increase in TC activity in the Eastern North Pacific basin which comprises both the eastern and central Pacific subregions. With the passage of the remnants of Hurricane Felicia that resulted in some significant rainfall and flooding, the state of Hawaii experienced its first TC since Hurricane Iniki in 1992.

The Atlantic ITCZ was prominently featured in the news, as strong convective activity associated with it was cited as one possible factor in the tragic downing of Air France Flight 447 some 300 miles off the coast of Brazil in early June. In the Indian Ocean, the 2009 season had a neutral to weak Indian Ocean Dipole (IOD) signal after an unprecedented three-consecutive positive IOD signals from 2006 to 2008.

This tropics chapter consists of six sections: (1) ENSO and the Tropical Pacific; (2) Tropical Intraseasonal Activity; (3) TC activity for the 2009 season in seven basins: the North Atlantic, Eastern North Pacific, Western North Pacific, North Indian and South Indian Oceans, Southwest Pacific, and Australia; (4) ITCZ behavior in the Pacific and Atlantic basins; (5) the IOD; and (6) a section on TC Heat Potential, previously in the Oceans chapter, helps summarize the section for TCs from an ocean heat perspective.

b. ENSO and the tropical Pacific—M. Halpert, G. D. Bell, and M. L'Heureux

1) Oceanic conditions

ENSO is a coupled ocean-atmosphere phenomenon centered in the equatorial Pacific Ocean. ENSO features two opposing phases, El Niño and La Niña, which are responsible for considerable interannual climate variability in the global tropics and the mid-to-high latitudes. NOAA defines these ENSO phases using the Niño 3.4 index, which reflects area-averaged SST anomalies in the east-central equatorial Pacific between 5°N and 5°S and 170°W and 120°W. El Niño occurs when the three-month running mean value of the Niño 3.4 index (called the Oceanic Niño Index—ONI) is greater than or equal to +0.5°C; La Niña occurs when the ONI is less than or equal to −0.5°C.

Both La Niña and El Niño occurred during 2009, with La Niña continuing during January–March (JFM) and El Niño prevailing from June through the end of the year (Fig. 4.1). December–February (DJF) in the 2008/09 season represented the second consecutive DJF period with La Niña conditions. During JFM, the weekly Niño 3.4 index ranged from −0.5°C to −1.1°C (Fig. 4.1). La Niña ended abruptly in early April as SST anomalies increased rapidly, with anomalous warming continuing during April–June, leading to the development of El Niño in late June. El Niño remained weak through September. Rapid strengthening during October followed and the Niño 3.4 index more than doubled to +1.5°C. Additional strengthening occurred during November and December, with the Niño 3.4 index averaging +1.8°C during December. The ONI value for October–December (OND) reached +1.5°C, which the NOAA's CPC considers to be a strong episode.

The anomalous seasonally-averaged surface and sub-surface temperature patterns associated with ENSO during 2009 are summarized in Figs. 4.2 and 4.3, respectively. During DJF, the equatorial cold tongue in the eastern Pacific Ocean was very well-defined and extended westward to the international date line (Fig. 4.2a). This feature was also stronger than average, with negative SST anomalies of −1°C evident in parts of the central and eastern Pacific (Fig. 4.2b). The pattern of sub-surface temperature anomalies during the period reflected an increased slope of the thermocline (thick black line) with positive sub-surface temperature anomalies and a deeper-than-normal thermocline in the western Pacific and negative anomalies and a shallower-than-normal

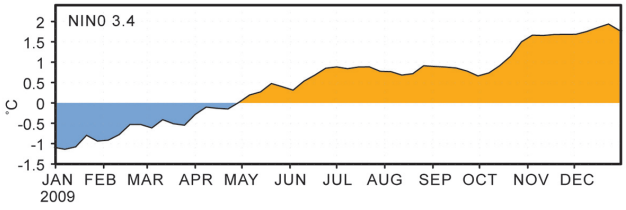

Fig. 4.1. Time series of weekly SST anomalies (°C) in the Niño-3.4 region (5°N–5°S, 170°–120°W). Anomalies are departures from the 1971–2000 weekly adjusted OI climatology of Smith and Reynolds (1998).

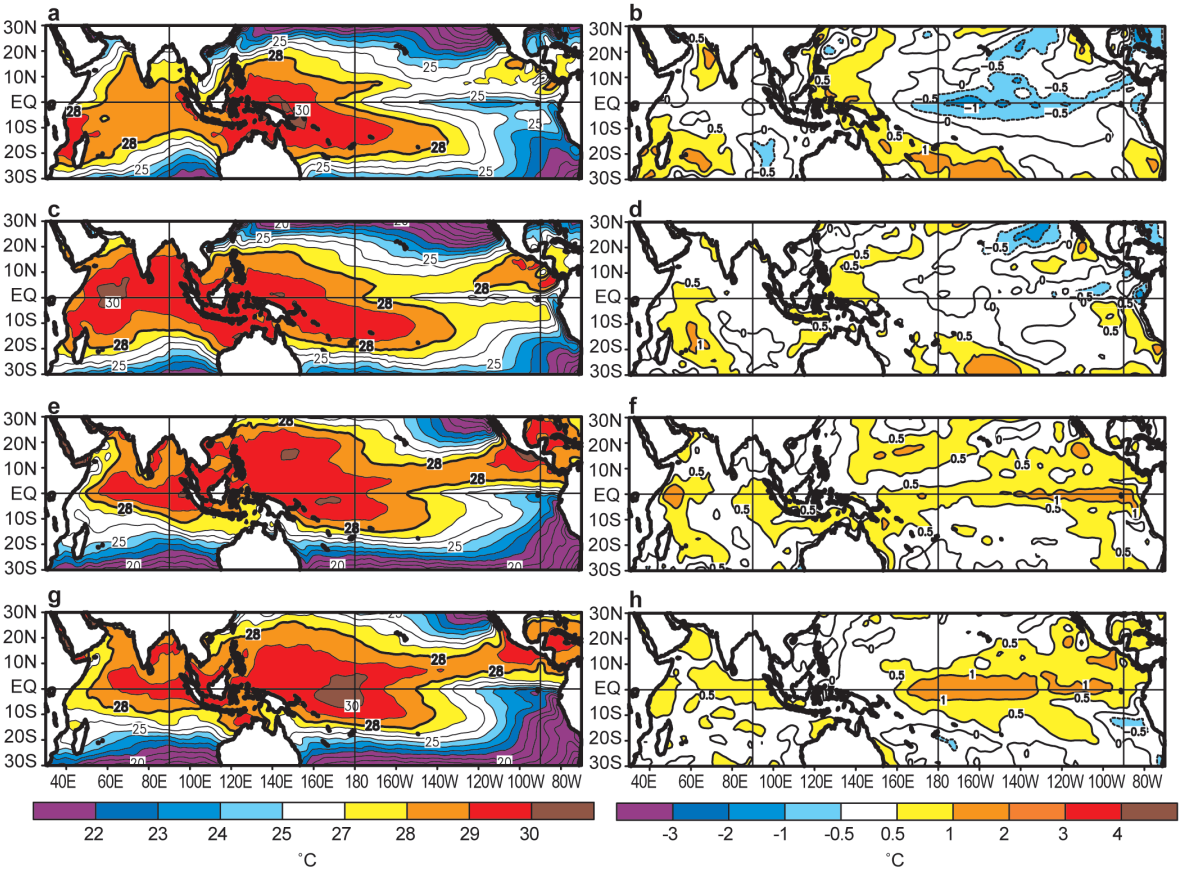

Fig 4.2. Seasonal SST (left) and anomaly (right) for (a), (b) DJF 2008/09, (c), (d) MAM 2009, (e), (f) JJA 2009 and (g), (h) SON 2009. Contour interval is 1°C, with the 0.5°C anomaly contour included. Anomalies are departures from the 1971–2000 seasonal adjusted OI climatology of Smith and Reynolds (1998).

thermocline in the east-central and eastern Pacific (Fig. 4.3a). These conditions are consistent with La Niña.

During March–May (MAM), surface (Figs. 4.2c, 4.2d) and subsurface ocean temperatures (Fig. 4.3b) returned to near-average across the eastern equatorial Pacific. Beginning in April, periodic westerly wind bursts over the western Pacific initiated equatorial oceanic Kelvin waves (section 4c, Fig. 4.7). During both June–August (JJA) and September–November (SON) (Figs. 4.3c, 4.3d) these Kelvin waves were associated with a deepening of the oceanic thermocline in the central and eastern Pacific and with a corresponding increase in subsurface ocean temperatures. At the same time, positive SST anomalies developed across the central and eastern part of the basin as El Niño developed and strengthened (Figs. 4.2f, 4.2h). Within the Niño 3.4 region, the dramatic increase in SSTs during October and early November was also associated with a strong oceanic Kelvin wave. By December 2009, SSTs were more than 2.0°C above average over large parts of the equatorial Pacific between 175°W and 90°W, with the warmest total SSTs (> 30°C) centered near the international date line.

2) Atmospheric circulation

Although La Niña was short-lived and modest in amplitude, its impacts on the patterns of tropical convection and atmospheric winds were pronounced (Fig. 4.4). For example, convection during DJF 2008/09 was suppressed over the central and west-central equatorial Pacific (brown shading) and enhanced over Indonesia and the far western Pacific (green shading). This pattern reflected a westward retraction of the equatorial convection toward the western Pacific and a disappearance of convection from the central Pacific. These conditions, combined with equatorial low-level easterly wind anomalies (Fig. 4.4a) and upper-level westerly wind anomalies (Fig. 4.4b), were associated with an enhanced Walker circulation typical of La Niña. Additional La Niña impacts were seen in the subtropics of both hemispheres, where upper-level cyclonic anomalies flanked the region of suppressed convection over the central Pacific.

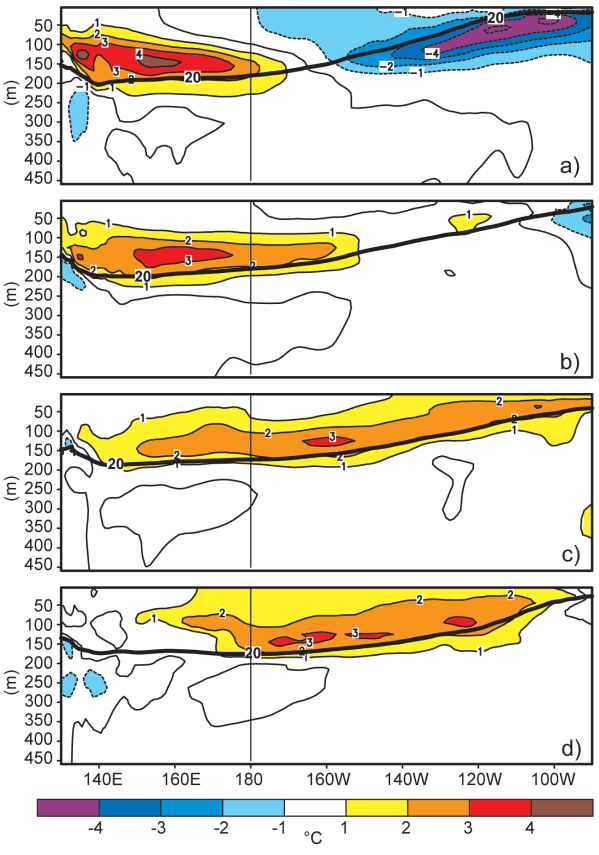

Fig 4.3. Equatorial depth-longitude section of ocean temperature anomalies (°C) averaged between 5°N and 5°S during (a) DJF 2008/09, (b) MAM 2009, (c) JJA 2008, and d) SON 2008. The 20°C isotherm (thick solid line) approximates the center of the oceanic thermocline. The data are derived from an analysis system that assimilates oceanic observations into an oceanic GCM (Behringer et al. 1998). Anomalies are departures from the 1971–2000 period monthly means.

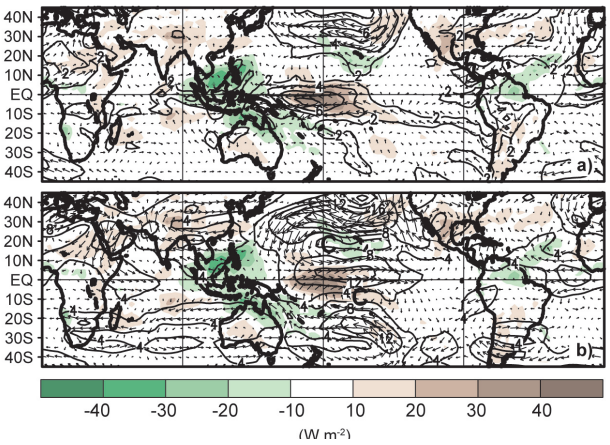

Fig. 4.4. (a) Anomalous 850-hPa wind vector and speed (m s^{-1}) and anomalous OLR (shaded, W m^{-2}) during DJF 2008/09 and (b) anomalous 200-hPa wind vector and speed (m s^{-1}) and anomalous OLR (shaded, W m^{-2}) during DJF 2008/09. Anomalies are departures from the 1979–95 period monthly means.

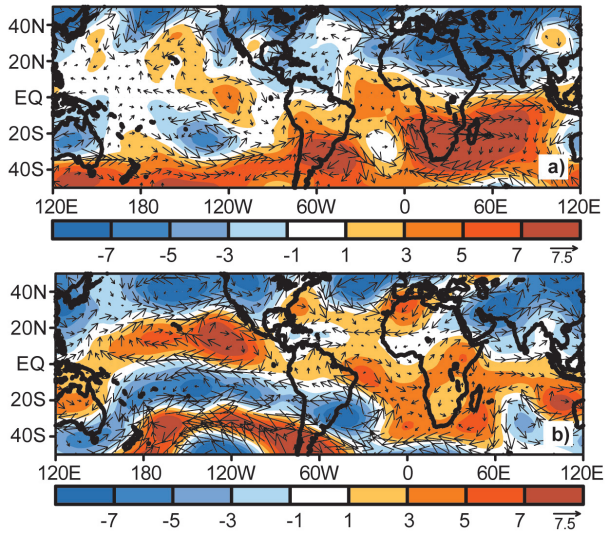

Fig. 4.5. Anomalous 200-hPa streamfunction (shading, x 10^6 m^2 s^{-1}) and wind vectors (m s^{-1}) during (a) JJA 2009 and (b) OND 2009. Anomalous ridges are indicated by positive values (red) in the NH and negative values (blue) in the SH. Anomalous troughs are indicated by negative values in the NH and positive values in the SH. Vector scale is to right of color bar. Anomalies are departures from the 1971–2000 period monthly means.

This anomaly pattern featured a retraction of the mean subtropical ridges in both hemispheres toward the western Pacific. In the Northern Hemisphere, it also reflected a westward retraction of the East Asian jet stream and below-average jet stream winds east of the date line. These conditions dissipated during MAM as La Niña ended.

El Niño developed during JJA and produced discernible impacts on the upper-level circulation (Fig. 4.5a) in a manner consistent with past episodes (Chelliah and Bell 2004). Prominent features of El Niño during this period included an anomalous zonal wave-1 pattern of 200-hPa streamfunction anomalies in the subtropics of both hemispheres. This pattern featured weak anticyclonic circulation anomalies over the central Pacific Ocean in both hemispheres and relatively stronger cyclonic anomalies extending eastward from the Americas to Australasia. Associated with this pattern, westerly wind anomalies between 30°S and 40°S reflected a strengthening and eastward extension of the mean wintertime jet stream over the South Pacific Ocean. Similar anomaly patterns were also evident during August–October (ASO), which led to a suppression of hurricane activity across the Atlantic basin (see section 4d2) and to stronger hurricane seasons in both the central (see sidebar article) and eastern Pacific (see section 4d3) sub-basins.

El Niño impacts on the 200-hPa circulation were especially pronounced during OND (Fig. 4.5b), with well-defined anticyclonic anomalies evident in the subtropics of both hemispheres over the central equatorial Pacific. In the Northern Hemisphere, strong westerly wind anomalies over the North Pacific between 20°N and 30°N reflected a pronounced eastward extension of the East Asian jet stream and an eastward shift of the mean jet exit region toward the eastern Pacific. North of the jet, the typical El Niño-related pattern of cyclonic anomalies was also evident. Along with these impacts, the extratropical anomaly patterns during both October and December also reflected record negative phases of the Arctic Oscillation (AO).

3) ENSO TEMPERATURE AND PRECIPITATION IMPACTS

During DJF 2008/09 La Niña impacted global precipitation patterns in a manner consistent with past cold episodes (Ropelewski and Halpert 1989). These impacts included suppressed convection across the central equatorial Pacific and above-average rainfall across much of the Maritime Continent (Indonesia, Philippines, Malaysia, and Borneo), which extended to the northernmost portions of Australia (Fig. 4.4a). In addition, above-average rainfall was observed in northeastern Brazil. Similar anomalies were also observed during DJF 2007–08 in association with La Niña (L'Heureux et al. 2009).

In the United States, La Niña contributed to drier than average conditions across the South during DJF 2008/09 and to increased precipitation in the northern Rockies and the Ohio and Tennessee Valleys. Temperatures over the United States were also generally consistent with La Niña, with below-average temperatures across the northern part of the country and above-average temperatures across parts of the South.

By the end of the year, the patterns of precipitation typically associated with El Niño (Ropelewski and Halpert 1987) were observed over parts of the world. These included above-average precipitation in the central equatorial Pacific and southeastern South America and below-average precipitation in parts of Indonesia and the Amazon Basin. Enhanced storminess and precipitation were observed across the southeastern United States in association with the anomalous East Asian jet stream.

c. Tropical intraseasonal activity—J. Gottschalck and G. D. Bell

The MJO (Madden and Julian 1971, 1972, 1994) is a leading climate mode of tropical convective variability that occurs on intraseasonal time scales. The convective anomalies associated with the MJO often have the same spatial scale as ENSO, but differ in that they exhibit a distinct eastward propagation and generally traverse the globe in 30–60 days. The MJO can strongly affect the tropical and extratropical atmospheric circulation patterns and sometimes produces ENSO-like anomalies (Mo and Kousky 1993; Kousky and Kayano 1994; Kayano and Kousky 1999). The MJO is often quite variable in any given year, with periods of moderate-to-strong activity sometimes followed by little or no activity. Overall, the MJO tends to be most active during neutral and weak ENSO periods and is often absent during strong El Niño events (Hendon et al. 1999; Zhang and Gottschalck 2002; Zhang 2005).

The MJO is seen by continuous propagation of 200-hPa velocity potential anomalies around the globe. A time-longitude section of this parameter shows four periods during 2009 with MJO activity

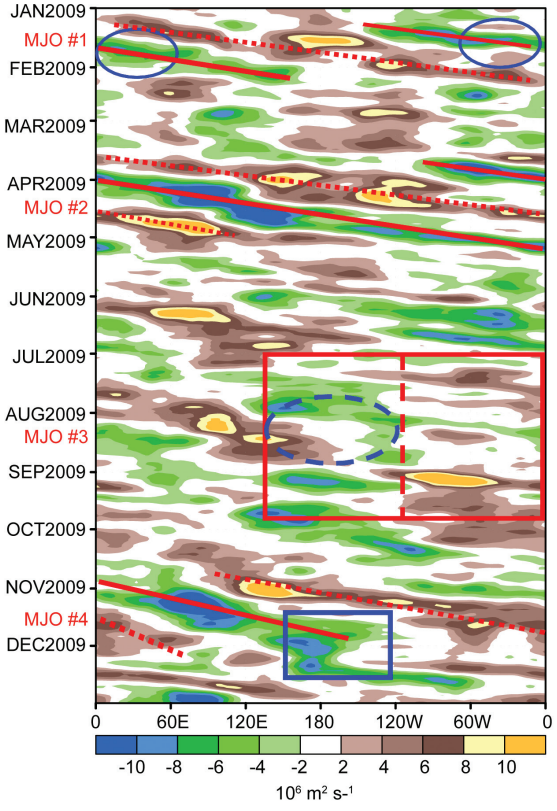

FIG. 4.6. Time-longitude section for 2009 of anomalous 200-hPa velocity potential (x 10^6 m^2 s^{-1}) averaged between 5°N-5°S. For each day, the average anomaly for the previous 120 days is removed prior to plotting. Green (brown) shading highlights likely areas of anomalous divergence and rising motion (convergence and sinking motion). Red lines highlight the main MJO episodes. Anomalies are departures from the 1971–2000 base period daily means.

(Fig. 4.6). These include four MJO periods depicted in Fig 4.6 as follows: (1) moderate activity during January (labeled MJO #1), (2) strong activity from mid-March to early May (MJO #2) (3) intraseasonal variability during July and August which partly reflected the MJO (MJO #3) and (4) strong activity from late October to mid-December (MJO #4).

During the first half of January, a combination of the MJO and background La Niña conditions produced enhanced rainfall across Indonesia (indicated by negative velocity potential anomalies and anomalous upper-level divergence) and a stronger than normal South Pacific Convergence Zone (SPCZ) (not shown). During the remainder of January, very wet conditions were observed across portions of equatorial South America and Africa as this upper-level divergence shifted eastward (blue circles on Fig. 4.6). During April even stronger MJO activity produced anomalous upper-level divergence and increased tropical rainfall from the Indian Ocean across Indonesia into the western Pacific.

From late July to mid-August, several forms of intraseasonal variability [including a faster propagating atmospheric Kelvin wave (Wheeler and Kiladis 1999; Wheeler and Weickmann 2001) and the MJO] contributed to an eastward shift of positive velocity potential anomalies and anomalous upper-level convergence from Indonesia to the central Pacific Ocean (Fig. 4.6, dashed blue circle). This shift acted to increase tropical activity in the Atlantic basin during an otherwise below average season, as demonstrated by development of TCs Ana, Bill, and Claudette (see section 4d2). This observation is consistent with past studies showing that conditions are more favorable for tropical development in the Atlantic basin when upper-level convergence prevails over the western Pacific Ocean to near the international date line and upper-level divergence dominates the western hemisphere (Mo 2000; Maloney and Hartmann 2000). A similar anomaly pattern during late October and early November was more clearly linked to strong MJO activity, which offset the El Niño signal and allowed for a rare late-season hurricane (Ida) to form over the Caribbean Sea; Ida was the only storm of the season to form in the Caribbean.

Opposite patterns of anomalous velocity potential were evident during both July and September (red boxes in Fig. 4.6). During September, these conditions were associated with El Niño, and contributed to a significant increase in vertical wind shear over the Atlantic basin (Fig. 4.16b) and to suppressed Atlantic hurricane activity.

The strong MJO activity during late October through early December also produced extratropical impacts. As the MJO shifted eastward across the western and central Pacific, the associated anomalous upper-level divergence and enhanced convection became superimposed upon the El Niño signal (Fig. 4.6, blue box) and acted to strengthen and extend eastward the East Asian jet stream. During mid-December, this jet stream undercut a persistent and strong upper-level ridge over western North America, allowing very wet and stormy conditions to affect California.

Between August and December, significant intraseasonal variability was also evident across the Pacific Ocean in association with three equatorial oceanic Kelvin waves (Fig. 4.7). The first two of these waves were initiated in early August and mid-September, in response to westerly wind events operating on a faster time scale than that of the MJO. The second wave traversed the eastern Pacific Ocean during late October and November and produced exceptionally large increases in anomalous oceanic heat content. This wave also contributed to the rapid increase in SSTs in the Niño 3.4 region during late October (Fig.

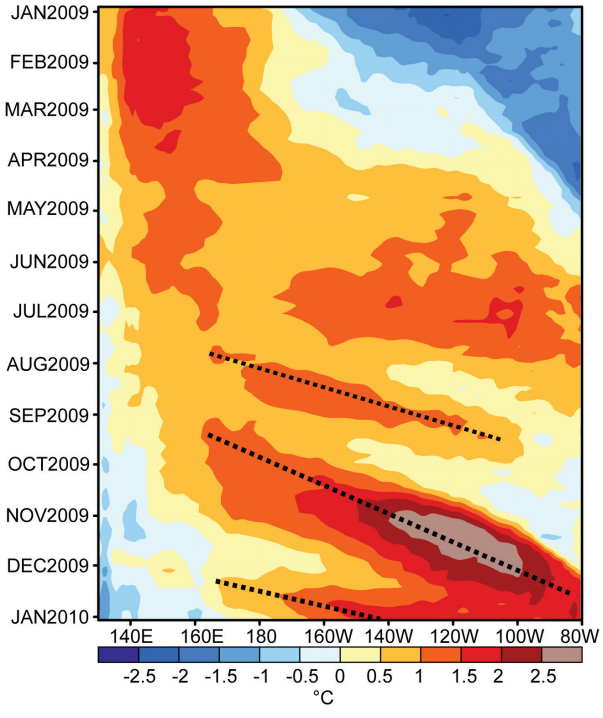

Fig. 4.7. Time-longitude section for 2009 of the anomalous upper ocean (0-300 m) heat content (°C) averaged between 5°N-5°S. Blue (yellow/red) shading indicates below (above) average heat content. The downwelling phases (dotted lines) of equatorial oceanic Kelvin waves are indicated. Anomalies are departures from the 1982–2004 base period pentad means.

4.1) and to large SST increases along the west coast of equatorial South America in early December. The third major Kelvin wave of the year was initiated over the western Pacific during December. This wave was triggered by a westerly wind burst linked to the MJO and reinforced the anomalously warm sub-surface waters in the central Pacific.

d. Tropical cyclones

1) Overview—H. J. Diamond

Global tallying of TC numbers is always challenging, and involves more than simply adding up basin totals, as some storms cross basin boundaries, some of the basins overlap, and multiple agencies are involved in tracking and forecasting TCs. Averaged across all seven TC basins, the 2009 season (2008/09 in the Southern Hemisphere) saw a below normal (1981–2000 base) number of tropical or named storms (NS) [≥ 34 kt] and a below-average number of hurricanes/typhoons/cyclones (HTC) [≥ 64 kt] and major HTCs [≥ 96 kt]. Globally, 90 NSs[1] developed during 2009 (7 below average) and 42 became HTCs (13 below average). Of these, 16 (compared to 26 in 2006, 18 in 2007, and 20 in 2008) attained major/intense status (global average is 25.4). Globally, the 2009 season was the least active since 2006.

From the standpoint of TC numbers, the 2009 season was above average in only one basin, the Eastern North Pacific which comprises both the eastern and central Pacific hurricane sub-regions. The season was below average in the North Atlantic Ocean and near to slightly below average in the remaining five basins, which are the Western North Pacific, the North Indian Ocean, the South Indian Ocean, the Southwest Pacific, and the Australian region

El Niño's emergence in June led to only the second below-normal Atlantic hurricane season (along with 1997) since 1995. El Niño also contributed to a sharp increase in hurricane activity across the central and eastern North Pacific. The re-emergence of above-normal activity in the Central Pacific sub-basin is highlighted in the chapter's sidebar article.

Despite a well below average Accumulated Cyclone Energy (ACE) Index value in the North Indian Ocean, the three systems that did make landfall ranked among the wettest ever observed in India and Bangladesh. For the Southwest Pacific the season had its latest start since 2001, with its first NS delayed until late January. Nonetheless, 2009 was that basin's most active season since 2006.

2) Atlantic basin—G. D. Bell, E. S. Blake, T. B. Kimberlain, C. W. Landsea, R. J. Pasch, J. Schemm, and S. B. Goldenberg

(i) Seasonal activity

The 2009 Atlantic hurricane season produced nine NSs, of which three became hurricanes (Hs) and two became major hurricanes (MHs). The 1950–2000 averages are 11 NSs, 6 Hs, and 2 MHs. The reduced activity during 2009 reflected fewer, shorter-lived, and generally weaker storms compared to most seasons since the high-activity era for Atlantic hurricanes began in 1995 (Goldenberg et al. 2001). As a result, the ACE index (Bell et al. 2000) for 2009 was 60% of the median (Fig. 4.8), and approximately one-third of the seasonal average since 1995 (which is 165% of the long-term median). Based on NOAA's classification[2], 2009 was only the second (along with 1997) below-normal Atlantic hurricane season since 1995.

One NS (Claudette in the Florida Panhandle) made landfall in the United States during 2009, and Ida brought tropical storm force winds to the northern U.S. Gulf Coast before becoming extratropical prior to making landfall. Only one NS (Ida) formed in the Caribbean Sea, making landfall as a hurricane in Nicaragua before weakening to a tropical depression (TD) while crossing southeastern Honduras. Tropical Storm[3] (TS) Erika passed through the northern Caribbean Islands while weakening, and H Bill brushed Nova Scotia and Newfoundland (Cangialosi and Avila 2010).

This represents a sharp decrease in the number of landfalling NSs compared to 2008, when the nations in and surrounding the Caribbean Sea were severely impacted by four NSs and four Hs, and the continental United States was struck by three NSs and three Hs.

(ii) SSTs

For the August–October (ASO) climatological peak months of the Atlantic hurricane season, SSTs were above average throughout the Main Development Region (MDR), defined as the Caribbean Sea and tropical Atlantic Ocean between 9.5°N and 21.5°N (Shapiro and Goldenberg 1998). The largest SST departures (+0.5°C to +1.0°C) were found across

[1] It should be noted that in the Western North Pacific there were an additional nine unnamed tropical depressions recorded by the Japan Meteorological Agency not included in this total.

[2] See http://www.cpc.noaa.gov/products/outlooks/background_information.shtml

[3] A TS is equivalent to an NS

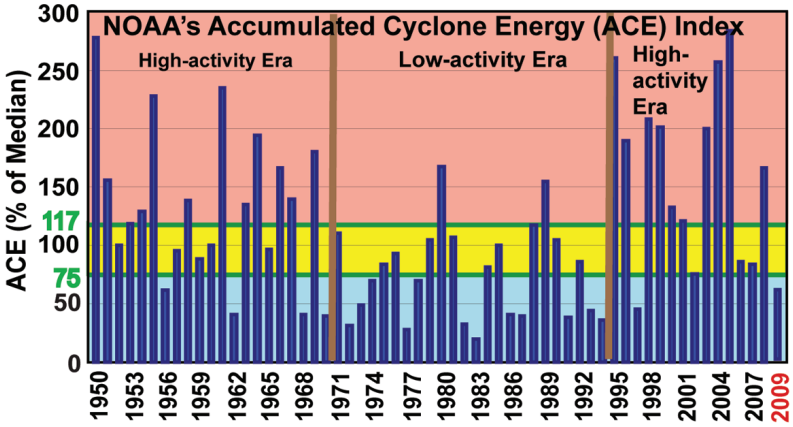

Fig. 4.8. NOAA's ACE index expressed as percent of the 1950-2000 median value (87.5×10^4 kt^2). ACE is a wind energy index that measures the combined strength and duration of the NSs. ACE is calculated by summing the squares of the 6-hr maximum sustained wind speed (kts) for all periods while the named storm has at least TS strength. Pink, yellow, and blue shadings correspond to NOAA classifications for above-, near-, and below-normal seasons, respectively. Brown lines separate high- and low-activity eras.

the south-central and eastern MDR (Fig. 4.9a). The ASO area-averaged departure for the entire MDR was +0.50°C, which is tied for seventh warmest since 1950 (Fig. 4.9b).

This warmth reflects three main factors: (1) the warm phase of the Atlantic Multidecadal Oscillation (AMO) (Enfield and Mestas-Nuñez 1999), which accompanied the 1995 transition to the active Atlantic phase of the tropical multidecadal signal (Bell and Chelliah 2006); (2) reduced mixing and reduced evaporation from the ocean surface in association with weaker northeasterly trade winds (anomalous southwesterly flow) across most of the tropical Atlantic portion of the MDR (Fig. 4.10a); and (3) long-term trend (Santer et al. 2006). The reduced Atlantic hurricane activity during 2009, despite this anomalous warmth, is consistent with previous findings indicating that local atmospheric circulation anomalies, rather than local SST anomalies, are the dominant contributor to seasonal fluctuations in Atlantic hurricane activity (Shapiro and Goldenberg 1998; Bell and Chelliah 2006; Bell et al. 2006).

(iii) Atmospheric circulation

A mixed set of atmospheric conditions, some favorable and some unfavorable to TC activity, prevailed during ASO. Favorable conditions included westerly wind anomalies at 1000-hPa and below average sea level pressure over large portions of the MDR (Fig. 4.10a). The core of the African Easterly Jet (AEJ) was also shifted approximately 5° lat north of normal (black arrow, Fig. 4.10b), meaning the bulk of the African easterly wave energy (Reed et al. 1977) was often centered well within the MDR in an area of increased cyclonic shear (orange shading). This jet configuration favors stronger easterly waves and provides a cyclonic rotation to their embedded convective cells (Bell and Chelliah 2006).

Unfavorable conditions included exceptionally strong vertical wind shear (blue shading, Fig. 4.11) and anomalous upper-level convergence (Fig. 4.12) over the Caribbean Sea. These conditions were linked to an anomalously strong and persistent Tropical Upper Tropospheric Trough (TUTT, blue shading in Fig. 4.10c) over the Caribbean Sea. This TUTT produced a combination of anomalous upper-level westerly winds and low-level easterly winds (Fig 4.13a) which increases the vertical wind shear. The TUTT also suppressed the normal rising motion so

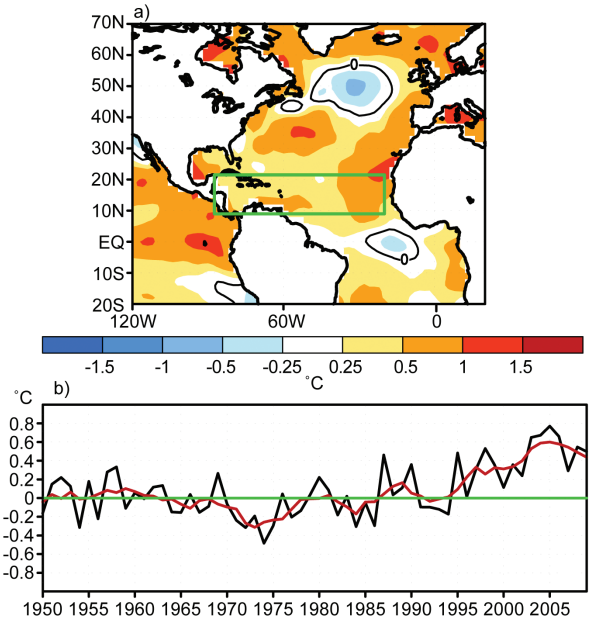

Fig. 4.9. (a) SST anomalies (°C) during Aug–Oct 2009. (b) Consecutive Aug–Oct area-averaged SST anomalies in the MDR. Red line shows the corresponding 5-yr running mean. Green box in a) denotes the MDR, which spans 9.5°N-21.5°N and 20.0°W-87.5°W. Anomalies are departures from the 1971–2000 monthly means.

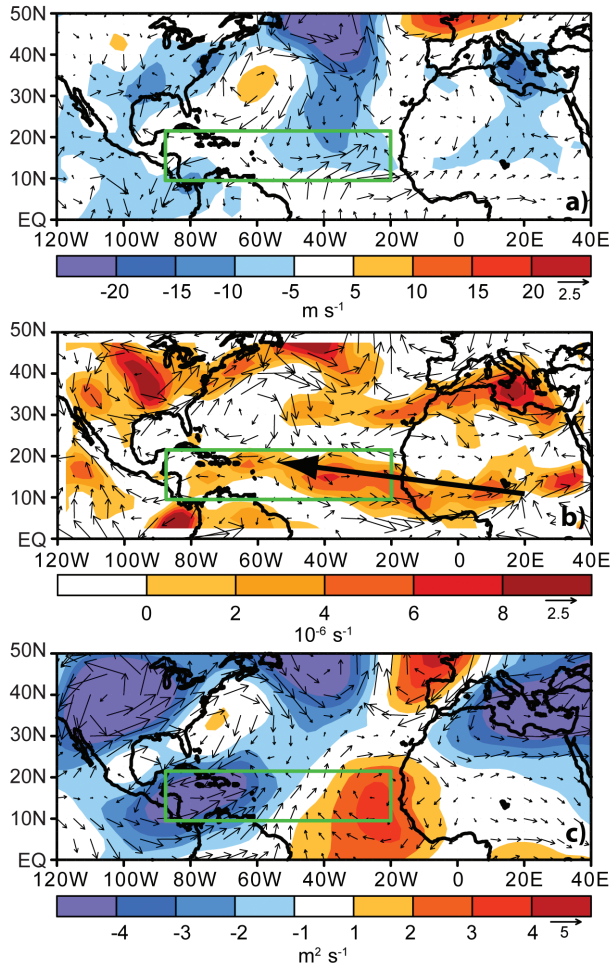

Fig. 4.10. Aug–Oct 2009: (a) 1000-hPa anomalous height (shading, m) and vector wind (m s^{-1}),(b) 700-hPa anomalous cyclonic relative vorticity (shading, x 10^{-6} s^{-1}) and vector wind, with thick arrow indicating the AEJ axis. (c) 200-hPa anomalous streamfunction (shading, x 10^6 m^2 s^{-1}) and vector wind. Green boxes denote the MDR. Vector scales are located right of color bars. Anomalies are departures from the 1971–2000 period monthly means.

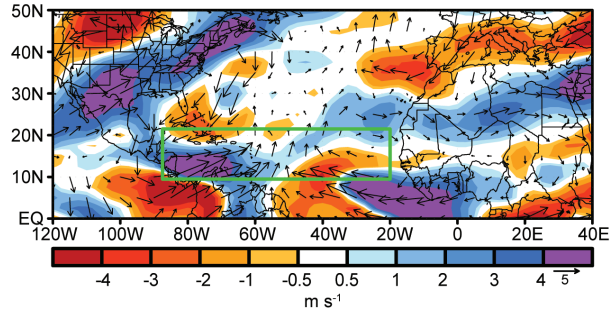

Fig. 4.11. Aug–Oct 2009: Anomalous 200-850 hPa vertical wind shear magnitude (m s^{-1}) and vectors. Green box denotes the MDR. Vector scale is located right of color bar. Anomalies are departures from the 1971–2000 period monthly means.

that only weak ascent prevailed throughout the MDR (Fig. 4.13b). In addition to suppressing the overall hurricane season strength, these conditions acted to decrease sharply the number of landfalling NSs in 2009 compared to 2008.

(iv) Links to global climate patterns

The regional atmospheric conditions and Atlantic TC activity during 2009 largely reflected two competing climate factors: El Niño and the ongoing active Atlantic phase of the tropical multidecadal signal (Bell et al. 2009). Across the tropical Pacific Ocean, the 200-hPa velocity potential and divergent wind anomalies during ASO (Fig. 4.12) were consistent with El Niño, as was an overall zonal wave-1 pattern of 200-hPa streamfunction anomalies in the subtropics of both hemispheres (Fig. 4.14). This pattern reflected enhanced subtropical ridges over the Pacific

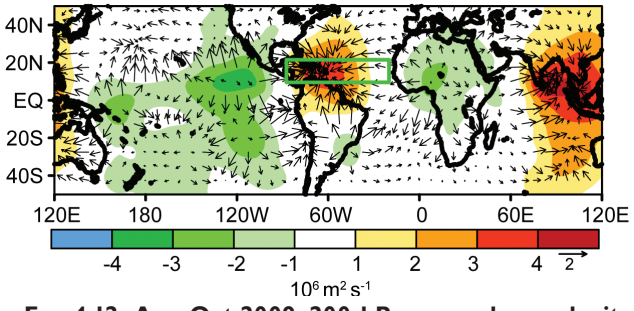

Fig. 4.12. Aug-Oct 2009: 200-hPa anomalous velocity potential (shading, x 10^6 m^2 s^{-1}) and divergent wind vectors (m s^{-1}). Vector scale is located right of color bar. Anomalies are departures from the 1971–2000 period monthly means.

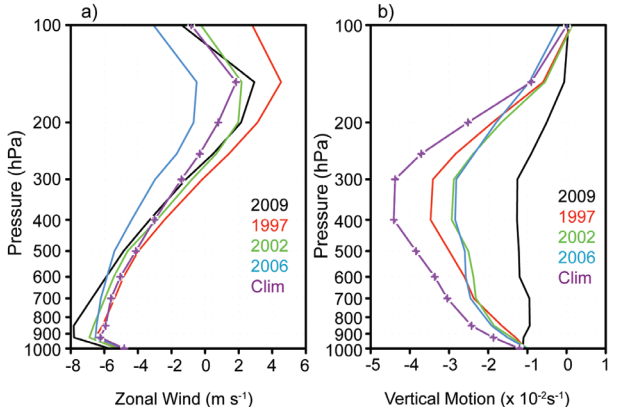

Fig. 4.13. Area-averaged conditions in the MDR during ASO for recent El Niño years: (a) total zonal wind (m s^{-1}), with negative (positive) values indicating easterly (westerly) winds and (b) total vertical motion (x 10^{-2} s^{-1}), with negative (positive) values indicating rising (sinking) motion. Climatology (Clim) is the 1971–2000 base period means.

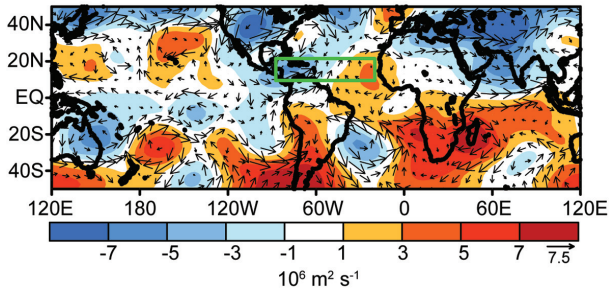

Fig. 4.14. ASO 2009: Anomalous 200-hPa streamfunction (shading, x 10^6 m^2 s^{-1}) and wind vectors (m s^{-1}). Anomalous ridges are indicated by positive values (red) in the NH and negative values (blue) in the SH. Anomalous troughs are indicated by negative values in the NH and positive values in the SH. Vector scale is located right of color bar. Anomalies are departures from the 1971–2000 period monthly means.

Ocean in both hemispheres, and weaker than average subtropical ridges throughout the remainder of the global subtropics.

Over the Caribbean Sea, regional aspects of this El Niño signal included the enhanced TUTT, stronger than average westerly winds at 200-hPa, increased vertical wind shear, and anomalous sinking motion, all of which overwhelmed the ongoing multidecadal signal and suppressed the 2009 Atlantic hurricane season. These conditions are opposite to those observed during 2008, when the combination of the high-activity era and La Niña contributed to an above normal Atlantic hurricane season (Bell et al. 2009).

(v) Conditions associated with the ongoing high-activity era in the tropical Atlantic

During the current high-activity era for Atlantic hurricanes, which began in 1995, two-thirds (10 of 15) of Atlantic hurricane seasons have been above normal, and only two have been below normal (Fig. 4.8). This elevated activity contrasts with the preceding low-activity era 1971–94, when one-half of the seasons were below normal and only three were above normal. During 1995–present, four of the five seasons not classified as above normal (1997, 2002, 2006, and 2009) can be linked to El Niño.

The transition to the current high-activity era was associated with a phase change in the tropical multidecadal signal, which reflects the leading modes of tropical convective rainfall variability and Atlantic SSTs occurring on multidecadal time scales (Bell and Chelliah 2006; Bell et al. 2007). This signal highlights the convectively-driven nature of the atmospheric anomalies across the central and eastern MDR, and links them to an east-west oscillation in anomalous convection between western Africa (Landsea and Gray 1992; Goldenberg and Shapiro 1996) and the Amazon Basin.

The combination of an enhanced West African monsoon and suppressed convection in the Amazon Basin was seen again during ASO (Fig. 4.12) and is known to be associated with an inter-related set of atmospheric anomalies typical of active hurricane seasons (Landsea et al. 1998; Bell et al. 1999, 2000, 2004, 2006, 2009; Goldenberg et al. 2001; Bell and Chelliah 2006; Kossin and Vimont 2007). These anomalies include enhanced low-level inflow into the West African monsoon region (Fig. 4.10a) and enhanced upper-level divergent outflow from that region (Fig. 4.12). They also include stronger upper-level ridges over both the eastern MDR and across the subtropical South Atlantic as seen in 2009 (Fig. 4.14), along with a stronger tropical easterly jet at 200 hPa.

Accompanying these conditions, the vertical wind shear (Fig. 4.15a) and 700-hPa zonal winds (Fig. 4.15b) in critical parts of the MDR have been much weaker since 1995 compared to the preceding low-activity era, and the 700-hPa relative vorticity has been cyclonic

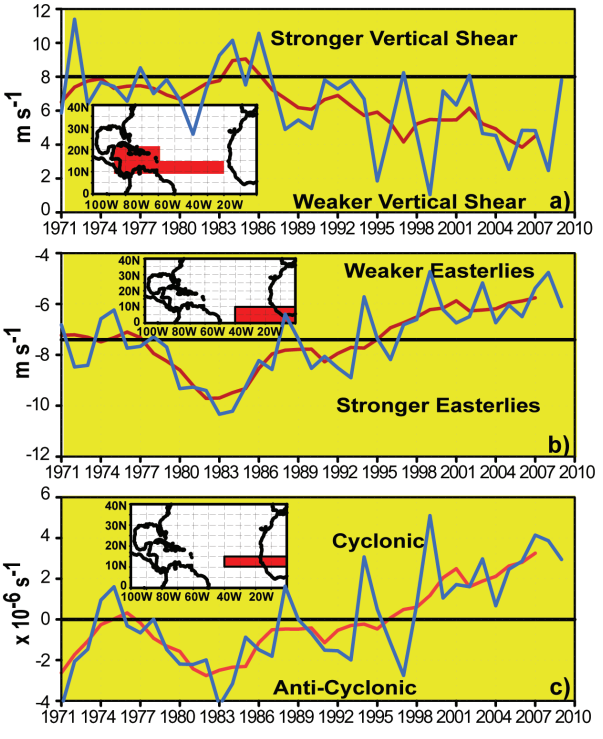

Fig. 4.15. Time series showing consecutive ASO values of area-averaged (a) 200-850 hPa vertical shear of the zonal wind (m s^{-1}), (b) 700-hPa zonal wind (m s^{-1}) and (c) 700-Pa relative vorticity (x 10^{-6} s^{-1}). Blue curve shows unsmoothed values, and red curve shows a 5-pt running mean of the time series. Averaging regions are shown in the insets.

rather than anticyclonic across the southern MDR (Fig. 4.15c). These latter two features were again present during ASO and are consistent with the more conducive AEJ described above.

As discussed by Bell and Chelliah (2006) and Bell et al. (2009), the above combination of conditions means that tropical storms can develop within the MDR from amplifying African easterly waves moving within the region of below-average pressure and increased cyclonic shear along the equatorward flank of the AEJ. In the absence of El Niño, these waves are also embedded within an extended region of weak vertical wind shear, which enables further intensification as they move westward over progressively warmer SSTs.

(vi) Intraseasonal variability in Atlantic hurricane activity

During 2009 intraseasonal variability in Atlantic hurricane activity resulted from a combination of the MJO and an atmospheric equatorial Kelvin wave (see section 4c). For example, six NSs including both MHs formed during 11 August to 7 September, and the third H of the season did not form until early November. During these more active periods, the MJO contributed to anomalous upper-level convergence over the central equatorial Pacific (Fig. 4.6). In mid-August an atmospheric Kelvin wave also contributed to this anomalous upper-level convergence. These conditions resulted in a more conducive pattern of vertical wind shear across the tropical Atlantic (Fig. 4.16a) similar to that described (Mo 2000). In contrast, only two NSs formed during most of September and October, a period when El Niño dominated the 200-hPa divergence signal (Fig. 4.12). Particularly impressive is the exceptionally strong vertical wind shear during September across most of the MDR (Fig. 4.16b).

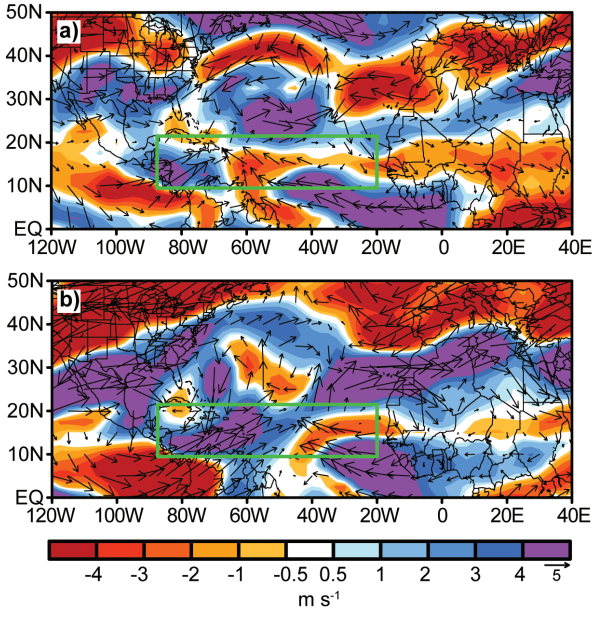

Fig. 4.16. Anomalous 200–850 hPa vertical wind shear magnitude (m s^{-1}) and vectors during (a) August 2009 and (b) September 2009. Green boxes denote the Main Development Region (MDR). Vector scale is located right of color bar. Anomalies are departures from the 1971–2000 period monthly means.

3) Eastern North Pacific (ENP) basin—D. H. Levinson, E. J. Gibney, J. Weyman, and M. C. Kruk

(i) Seasonal activity

The ENP basin is officially split into two separate regions for the issuance of warnings and advisories by NOAA's National Weather Service (NWS). NOAA's National Hurricane Center (NHC) in Miami, FL is responsible for issuing warnings in the eastern part of the basin that extends from the Pacific Coast of North America to 140°W, while NOAA's Central Pacific Hurricane Center (CPHC) in Honolulu, HI is responsible for issuing warnings in the Central North Pacific region between 140°W and the international date line. In this section analysis summarizing the tropical cyclone activity in both these warning areas will be presented using combined statistics, along with information specifically addressing the observed activity and impacts in the Central North Pacific (CNP) region.

The ENP hurricane season officially spans from 15 May to 30 November, although storms can develop outside of the official season, especially during El Niño enhanced hurricane seasons[4]. Hurricane and tropical storm activity in the eastern area of the basin typically peaks in September, while in the Central Pacific TC activity reaches its seasonal peak normally in August (Blake et al. 2009). Figure 4.17 shows the tracks of all of the observed TCs in the ENP and CNP in 2009. TC activity in the ENP started later than normal this past year, with the development of two systems in June (TD 01E during 10–18 June, and H Andres during 21–24 June), which was the first time since 1999 that no named storms formed during May. For the season as a whole, the number of NSs and MHs that developed were both slightly above their long-term means, while the number of Hs was

[4] TS Paka was the last TC to occur in December in the ENP basin when it developed in the Central Pacific region during 2–6 December1997.

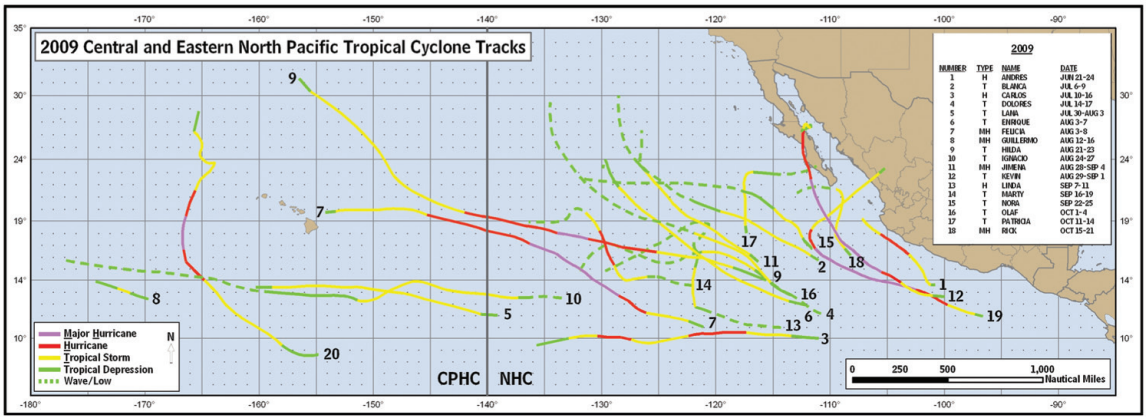

Fig. 4.17. The tracks of all TCs that occurred in the ENP and CNP basins (Source: NOAA's NHC and CPHC). Tracks are color-coded by intensity (wave/low, tropical depression, tropical storm, hurricane, major hurricane). Also shown is the delineation of the forecast area of responsibility at 140°W longitude between NOAA's NHC and CPHC.

near-normal. Primarily due to the development of an El Niño warm event during the boreal summer and early autumn in the equatorial Pacific in 2009, the hurricane season was above average in the ENP basin, with 20 NSs, 9 Hs, and 5 MHs (Fig. 4.18a). These values are at or above the 1971–2005 averages for the basin (16.2 NSs, 9.1 Hs, and 4.3 MHs).

Despite the overall above average activity in 2009 in terms of storm counts, the ACE Index (Bell et al. 2000; Bell and Chelliah 2006) was near-normal for the basin with a seasonal total of 106.1×10^4 kt^2, which was slightly below the 1971–2005 mean (126.3×10^4 kt^2), but higher than occurred during the previous two seasons (Fig. 4.18b).

A total of seven TCs were observed in the CNP region in 2009, three of which developed in the region and were officially named by the CPHC (TS Lana, TS Maka, and H Neki)[5], while three others propagated into the region from the east (Fig. 4.17) crossing the warning area boundary of 140°W (MH Felicia, MH Guillermo, and TS Hilda). Three TCs reached hurricane strength in the CNP warning area, one of which developed into a major hurricane (Neki). This was the largest number of TCs in the CNP since 1997, and well above the 1971–2005 average of 4–5 TCs[6]. The enhanced activity in the CNP was also likely a result of the influence of the El Niño warm event that developed during the hurricane season, which generated more TC activity west of 140°W (see sidebar).

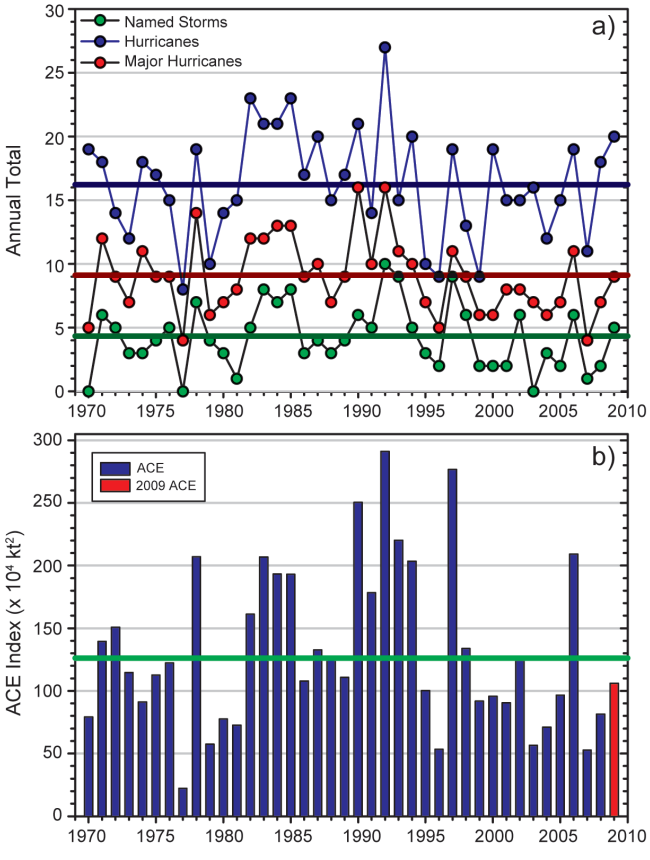

Fig. 4.18. Seasonal TC statistics for the ENP basin over the period 1970–2009: (a) number of NS, H, and MH and (b) the ACE Index (x 10^4 kt^2) with the seasonal total for 2009 highlighted in red. All time series shown include the corresponding 1971–2005 base period means for each parameter. (Source: International Best Track Archive for Climate Stewardship [IBTrACS].)

[5] A non-named TD (02C) was also noted during this period.

[6] NOAA's CPHC includes TDs in their climatological statistics for the CNP basin.

Since 1995, the number of NSs in the ENP basin has been near average, fluctuating about the long-term mean (Fig. 4.18a). However, the numbers of Hs and MHs have been generally below normal in most seasons, with above normal activity having occurred in only three seasons. NOAA has identified 9 of the 15 seasons in the ENP as being below normal during 1995–2009, with only the El Niño–influenced seasons of 1997 and 2006 producing above normal activity as measured by the ACE index. In contrast, enhanced activity was observed during the preceding 1970–94 period, which had 6 of 25 (24%) below normal seasons and 9 of 25 (36%) above normal seasons, as measured by the ACE index.

(ii) Environmental influences on the 2009 season

Seasonal TC activity (both frequency and intensity) in the ENP basin is influenced by several large-scale environmental factors in the basin, including SSTs, the vertical shear of the horizontal wind, the phase of the ENSO phenomenon in the equatorial Pacific, as well as the phase of the Quasi-Biennial Oscillation (QBO) in the near-equatorial lower stratosphere (Gray 1984; Shapiro 1989; Whitney and Hobgood 1997; Hobgood 2003). ENSO is known to strongly modulate both the SSTs and vertical wind shear on interannual time scales in the ENP basin (Whitney and Hobgood 1997). However, multidecadal fluctuations in ENP hurricane activity are less well understood but do show a strong inverse relationship to the phase of the tropical multidecadal mode and Atlantic hurricane activity (Bell and Chelliah 2006; Wang and Lee 2010).

Previous studies have documented that the occurrence of an El Niño typically favors an above-normal hurricane season, while La Niña (and neutral) conditions typically favor a below-normal hurricane season in the ENP (Irwin and Davis 1999; Frank and Young 2007; and Camargo et al. 2008). These ENSO impacts are modulated by the multidecadal signal, with the combination of a La Niña occurrence during an inactive hurricane era greatly increasing the probability of a below-normal season. During 2009, the transition from an ENSO neutral phase to an El Niño during the climatological peak of the hurricane season (ASO) resulted in above average SSTs (weekly and monthly SST anomalies of +0.4°C to +1.5°C) in the MDR[7].

Another significant environmental factor that likely enhanced the above-normal hurricane season in 2009 was anomalously below-average vertical wind shear between 200 hPa and 850 hPa in the MDR during the latter half of the hurricane season (Fig 4.19a). During the first half of the hurricane season (JJA), the wind shear anomalies were above average (exceeding 9–12 m s^{-1}), which suppressed tropical-cyclogenesis and inhibited intensification. Conditions changed considerably during the latter half of the season, when negative wind shear anomalies of 9–12 m s^{-1} were observed during SON (Fig. 4.19b). It is likely that the significantly weaker-than-normal shear late in the season enhanced TC intensification and as a result 2009 had an above average number of MHs in the ENP. The late season formation of MH Rick (15–21 October), which reached a maximum intensity of 155 kt Category (Cat-) 5 and was the second strongest ENP hurricane in the historical record (behind MH Linda in 1997, which had a peak intensity of 160 kt), as well as the development of MH Neki in the Central Pacific (18–26 October), were both indications of the weak wind shear during the peak months of the hurricane season.

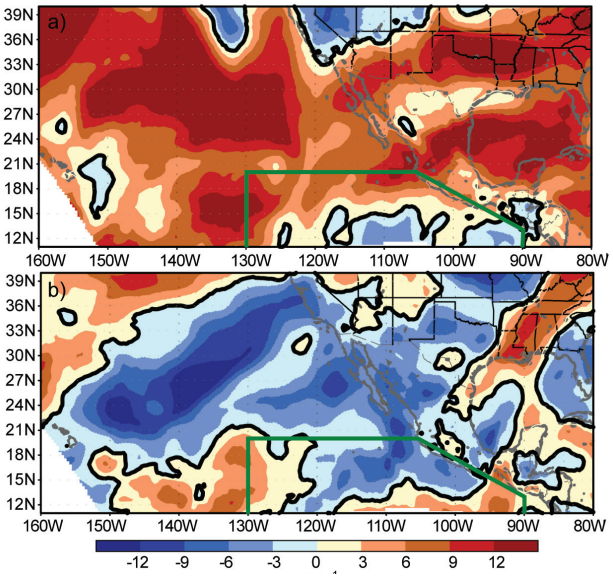

Fig. 4.19. The 200–850 hPa vertical wind shear anomalies (m s^{-1}) averaged over the following two periods in 2009: (a) June–August (JJA) and (b) September–November (SON), with anomalies determined relative to the 1979–2004 base period mean. The main development region for ENP hurricanes is the area delineated by the green polygon in both maps. (Source: North American Regional Reanalysis [NARR] dataset, provided by the NOAA National Operational Model Archive and Distribution System.)

[7] The MDR in the ENP covers the region delineated by the green boxes in Fig. 4.19 a-b; between10°N and 20°N and 90°Wand 130°W.

Several previous studies have shown statistically significant correlations between hurricane activity and the phase of the QBO (Gray 1984; Shapiro 1989; Whitney and Hobgood 1997). In the ENP basin, TCs have been shown to attain a higher intensity when the QBO is in its westerly phase, but there is also a corresponding decrease in the observed seasonal frequency (Whitney and Hobgood 1997). In June 2009, the phase of the QBO was westerly, as indicated by the zonally-averaged U-component winds at both 30-hPa and 50-hPa obtained from the NOAA CPC Climate Data Assimilation System (CDAS) dataset. In July, the zonal mean winds at 30-hPa shifted to easterly and remained from an easterly component for the remainder of the 2009 hurricane season. In contrast, the zonal winds at 50 hPa (not shown) remained from a westerly component for the entire hurricane season in the ENP. The effect of this split signal related to the phase of the QBO on the frequency and intensity of TC activity in the ENP is unclear. However, using data covering the 1963–1993 hurricane seasons, Whitney and Hobgood (1997) found that there are slightly fewer TCs over the ENP when the QBO is in its westerly phase, although these storms attained a slightly higher maximum intensity. Therefore, it is possible that the intensity of hurricanes in the ENP basin during the 2009 season may have been ehanced by the westerly phase of the QBO (based on the zonally-averaged wind at 50 hPa), as five major hurricanes formed during the season, which was the highest total since the 2006 season.

(iii) TC Impacts

Three TCs made landfall along the Pacific Coast of Mexico during the season (Cat-1[8] H Andres, Cat-2 H Jimena, and TS Rick). In comparison with climatology, the 2009 season was well above the 1951–2000 average of 1.34 landfalling TCs (Jauregui 2003). Along the Pacific Coast of Mexico, H Andres attained minimal hurricane strength (Cat-1 intensity) as it moved parallel to the coast in late June. Damage along Mexico's southwestern coast was minimal; however, heavy rains from Andres and its precursor disturbance flooded homes in a portion of Acapulco and resulted in the evacuation of about 200 people. Preliminary damage reports suggested that Andres was responsible for one fatality in Mexico.

Strong winds and heavy rainfall from H Jimena caused devastation as the storm crossed the Baja peninsula on 2–4 September, officially making landfall with sustained winds of 85 kt (Cat-2). Strong winds and heavy rains associated with Jimena caused widespread damage on the central and southern Baja California peninsula. The cities of Ciudad Constitución, Mulege, and Loreto were reported to be hard hit, as well as many of the smaller towns near the track of the storm's center. One fatality was reported—a drowning due to flash flooding in Mulege, Baja California del Sur—and 75% of homes were damaged in Puerto San Carlos. Severe damage also occurred to the agricultural sector. Approximately 400 hectares of citrus was lost and 80 hectares of greenhouses were destroyed by the storm. Total losses to the sector have been estimated to be at least $37.3 million (U.S.), with damages to infrastructure estimated at $12.5 million (U.S.).

On 21 October, TS Rick made landfall near Mazatlan with estimated maximum sustained winds of 50 kt, which was significantly weaker than the 155 kt the storm had reached at peak intensity. Preliminary reports suggested that Rick was responsible for two deaths in Mexico.

In the CNP, Felicia reached a maximum intensity of 120 kt (Cat-4) before it weakened significantly as it moved into the Central Pacific sub-basin and affected the main islands of Hawaii as a tropical depression in mid-August. Impacts from Felicia included heavy rainfall and localized flash flooding.

In October, the northwestern Hawaiian Islands were directly affected by MH Neki (Fig. 4.17, storm number 20), which caused the evacuations of researchers and scientists via a NOAA ship and a Coast Guard C-130 aircraft. Neki developed as a weak TC near 12°N, 130°W and slowly moved westward with little change in intensity. As it turned northwestward near 160°W, the system intensified, reaching a peak intensity of 105 kt (Cat-3). As its northern movement slowed, the storm crossed the archipelago near French Frigate Shoals and Necker Island as a strong TS (maximum sustained winds of 50–55 kt).

4) Western North Pacific (WNP) basin—S. J. Camargo

The 2009 season featured 28 TCs (including TDs) forming in the WNP. There were two (TS Maka and TD 02C) TCs which formed in the Central Pacific and crossed into the WNP. Of these 30 active TCs in the WNP, according to the Japan Meteorological Agency, nine additional TDs occurred in 2009. One of these TDs was named by the Philippine Atmospheric,

[8] Saffir-Simpson categories are used in this chapter, except for the Southwest Pacific and Australian regions which use the Australian system (see footnote in that section).

Geophysical and Astronomical Services Administration (PAGASA), which also named two other TDs (Bising and Crising) in the 2009 typhoon (TY) season. Twenty-five reached TS intensity (three of which were not named), 14 became TYs, and 5 reached super-typhoon (STY) intensity. In Fig. 4.20a the number of TSs, TYs, and STYs per year is shown for the period 1945–2009. The TC data used here is from the Joint Typhoon Warning Center (JTWC) best-track dataset for 1945–2008, and preliminary operational data for 2009, for the TCs forming in the WNP. Preliminary data for the storms forming in the Central Pacific region is from CPHC. Climatology is defined using the period 1971–2000.

The 2009 WNP TC season (see Fig. 4.20) started in May, with TYs Kujira and Chan-Hom. These were

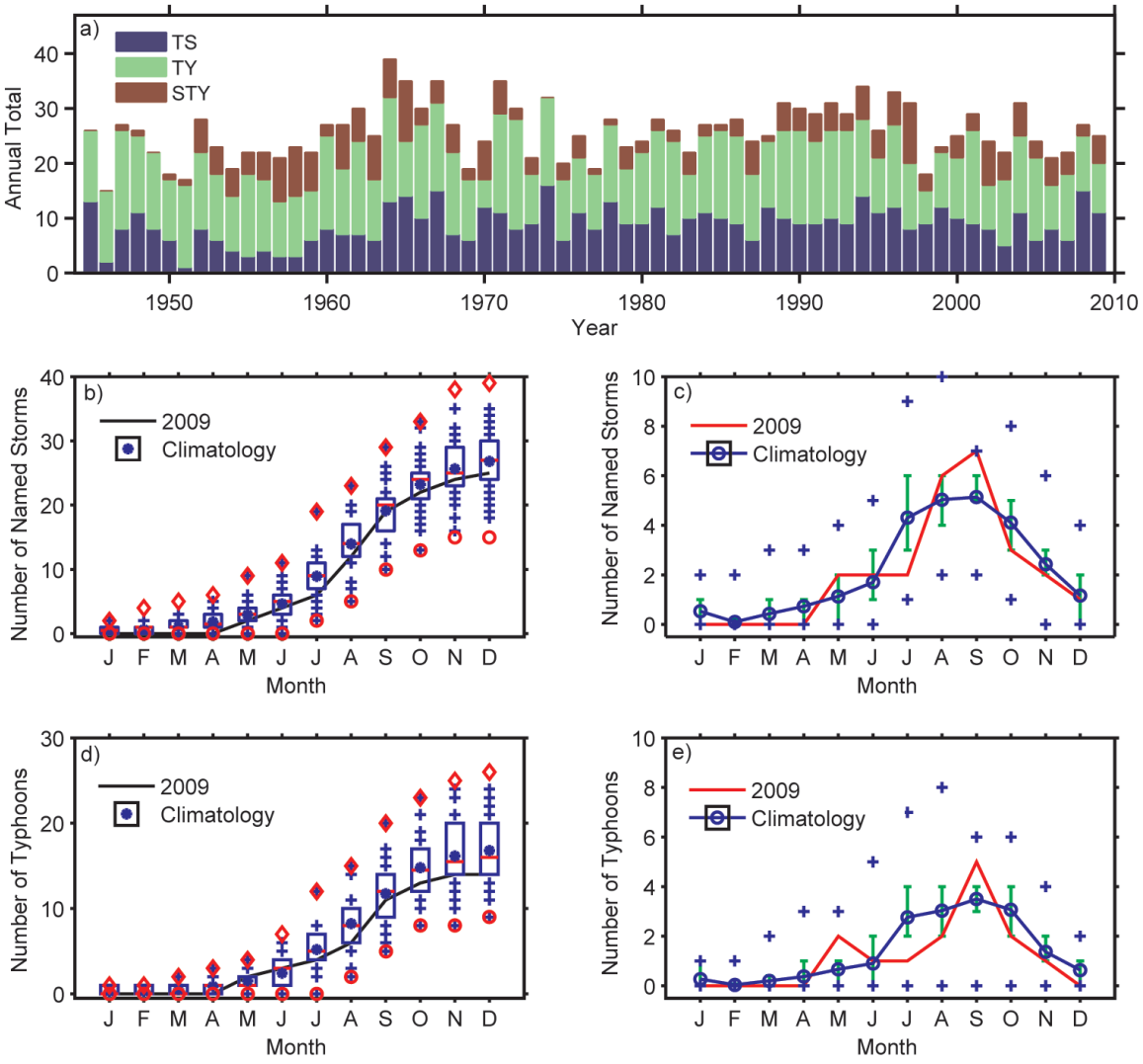

Fig. 4.20. (a) Number of TCs for the period 1945–2009. (b) Cumulative number of NSs per month: 2009 (black line), and climatology (1971–2000) shown as box plots [interquartile range: box, median: red line, mean: blue asterisk, values in the top or bottom quartile: blue crosses, high (low) records in the 1945–2008 period: red diamonds (circles)]. (c) Number of NSs per month in 2009 (black curve), mean climatological number of NS per month (blue curve), the blue plus signs denote the maximum and minimum monthly historical values (1945–2009) and green error bars show the interquartile range for each month. In the case of no error bars, the upper and/or lower percentiles coincide with the median. (d) Cumulative number of TYs: 2009 (black line), and climatology (1971–2000) shown as box plots. (e) Number of TY per month in 2009 (black curve), mean climatological number of TY per month (blue curve), the blue plus signs denote the maximum and minimum monthly historical values (1945–2009) and green error bars show the interquartile range for each month. (Source: 1945–2008 JTWC best-track dataset, 2009 JTWC preliminary operational track data.)

followed by TY Linfa and TS Nangka in June. July TC activity was below-normal, with only two TCs reaching TS intensity, TS Soudelor and TY Molave. On average for the month of July there are four NSs that develop, of which three reach TY intensity. In August, the TC activity was higher than in July, with three TSs (Goni, Etau, and Krovanh) and two TYs (Morakot and Vamco) forming in the WNP. In addition, two Central Pacific TCs, TS Maka and TD 02C crossed into the region. The most active month in TC genesis numbers was September, with one TD (Mujigae), two TSs (Dujuan and 18W), two TYs (Koppu and Ketsana), and three STYs (Choi-Wan, Parma and Melor) forming in the WNP. The seven NSs and three STYs that occurred in September tied the previous historical record of the number of NSs and STYs in that month. The TC activity in October was slightly below-average, with one TS (Nepartak), one TY (Mirinae), and one STY (Lupit) occurring in the basin. The last STY (Nida) of the 2009 season formed in November, along with two TDs (24W and 27W) and one non-named TS (25W). The season finished with the formation of TS 28W in early December.

The total number of TCs (30), NSs (25), and TYs (14) in 2009 were all below the median but equal to or above the 25th percentile of the climatological distributions (median: 30.5 TCs, 27 NSs, and 16 TYs, 25th percentile: 27 TCs, 24 NSs, and 14 TYs). The cumulative distributions of NSs (Fig. 4.20b) and TYs (Fig. 4.20c) show a slow season start, with the activity increasing in May, below-normal activity in July and August, and the high activity in September leading to slightly-below normal values for the season as a whole for NS and TY numbers. In contrast, the number of STYs in 2009 (five) was in the top quartile of the climatological distribution.

The ACE in the WNP (Fig. 4.21) reflects well the activity and number of TCs. The ACE value for the 2009 season was very near the climatological median (Fig. 4.21a), only slightly above the median, due to the very low value of ACE in July, which was not totally compensated by the high October and November ACE values. The May ACE was in the top quartile of climatology and the November ACE was very close to the 75th percentile of the climatology. July and October were complementary months, with the July ACE value being the 5th lowest and the October ACE being the 5th highest value in the historical record for the respective months. The ACE values of the two strongest storms in 2009, STYs Melor and Nida are in the top 5th percentile of the historical record and the climatological distribution. Ninety percent of the ACE in November is due to STY Nida, while 64% of the September ACE is due to STY Choi-Wan, and 37% of the October ACE is due to STY Melor.

There were 129 days with TCs and 122 days with NSs in 2009 in the WNP, both in the bottom quartile of the climatological distribution (medians 161.5 and 144.25 days, respectively). From these, there were 110 days with typhoons, slightly below the climatological median of 120.4 days. There were 22.25 days with intense TYs (categories 3–5), above the climatological median of 19.4 days. Climatologically, 74% (11%) of the TC days consist of days with (intense) TYs. In 2009 these ratios were much higher, 85.3% and 17.25%, respectively, pointing to a more frequent occurrence of intense and STYs in the 2009 TC season. The median lifetime of NSs in 2009 was 6.5 days, below the median lifetime of 8 days for all years. From the 25 NSs, 17 had a duration below the median,

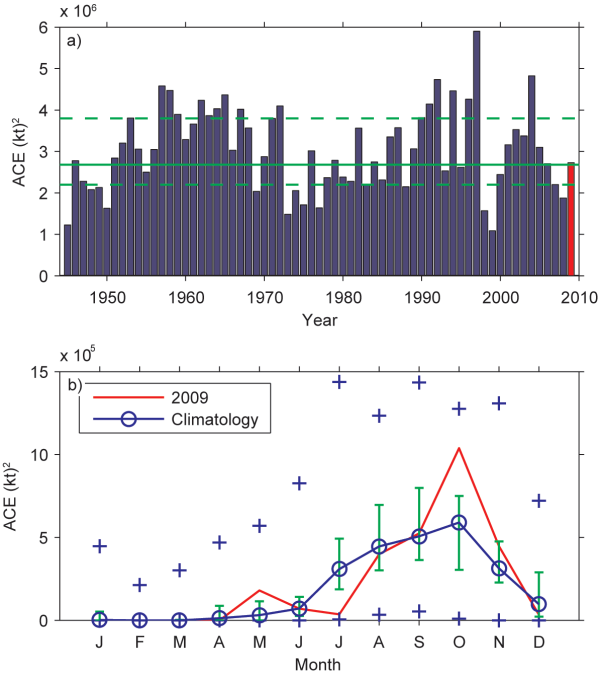

Fig. 4.21. (a) ACE Index per year in the Western North Pacific for the years 1945–2009. The solid green line indicates the median for the years 1971–2000 climatology, and the dashed green lines show the 25th and 75th percentiles. (b) ACE index per month in 2009 (red line) and the median in the years 1971–2000 (blue line), where the green error bars indicate the 25th and 75th percentiles. In the case of no error bars, the upper and/or lower percentiles coincide with the median. The blue plus signs (+) denote the maximum and minimum values during the period 1945–2009. (Source: 1945–2008 JTWC best-track dataset, 2009 JTWC preliminary operational track data.)

with 11 of those in the bottom quartile of the distribution. Only three TCs had a duration in the top quartile of the distribution, i.e., with lifetimes larger than 11.25 days, namely STYs Nida (11.75 days), Lupit (12.75 days), and Parma (17 days). STY Parma's very long lifetime of 17 days is in the top 2 percentile of the historical record.

The El Niño event in 2009 occurred in three phases. From June to September, it was a weak event and then ramped up in October to a moderate event. In December it was declared a strong event. There is a known relationship between WNP ACE and ENSO, with high values of ACE usually occurring in El Niño years, when the TCs tend to be long-lived and more intense (Wang and Chan 2002; Camargo and Sobel 2005; Camargo et al. 2007b). The 2009 ACE reflects the time evolution and strength of the El Niño event in 2009. In the early TC season, while ENSO was still weak, low (July) or average values of ACE occurred. Once the ENSO event became stronger, the ACE values also increased, especially in October and November, due to the occurrence of the five super-typhoons in the late September to November period. The 2009 median lifetime was below normal, and with exception of TY Chan-Hom, all the storms that had an above-normal lifetime occurred after late September, when the El Niño became a moderate to strong event. There was a flurry of TC activity in late September, when the MJO was active in the region, right before the ramp-up of the El Niño event. This would be in agreement with the hypothesis, discussed in Sobel and Camargo (2005), that TYs could help strengthen El Niño events.

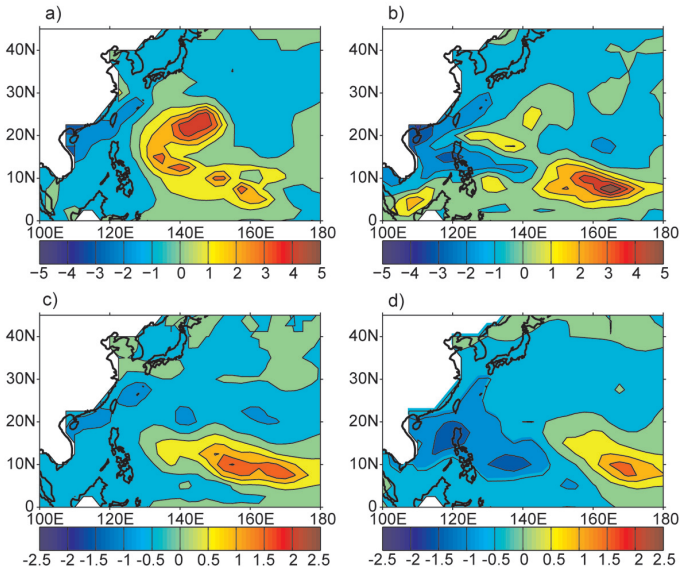

Fig. 4.22. Genesis potential index (Camargo et al. 2007b) anomalies for (a) JJA 2009; (b) SON 2009. El Niño genesis potential index anomaly composites (c) JJA; (d) SON. (Source: atmospheric variables - NCEP Reanalysis data, Kalnay et al. 1996; SST - Smith and Reynolds 2005.)

Emanuel's genesis potential index (GPI) (Camargo et al. 2007a) shows (Fig. 4.22) clearly the shift in the environmental conditions from the early (JJA) to the late (SON) season to more typical El Niño-like conditions. While the GPI anomalies for JJA do differ from the El Niño JJA composite pattern, the SON anomalies are very similar to the El Niño SON composite.

The mean genesis location (15.2°N, 140.5°E) in 2009 was shifted northwest of the climatological mean genesis positions (12.9°N, 143.5°E). While the mean track position (20.2°N, 134.9°E) is shifted slightly northward of the climatological mean (19.0°N, 134.2°E). These shifts are not consistent with the typical El Niño events, which tend to have a southeastward shift (Chan 1985; Chia and Ropelewski 2002). The late season (September to December) mean genesis position (14.2°N, 145.4°E) is more consistent with the typical shift in El Niño events.

Fourteen WNP TCs made landfall during 2009, which is just below the 1951–2000 median of 15[9]. Six systems made landfall as a TD (median is three), seven made landfall as TS (median is six), one struck as TY (median is four), and none as an STY (median is zero).

TY Morakot was a particularly catastrophic event for Taiwan, leaving 461 people dead and 192 others missing (most of whom were feared dead) with roughly $3.3 billion (U.S.) in damages. The storm produced record setting rainfall of 2777 mm, surpassing the previous record of 1736 mm set by TY Herb in 1996. The extreme amount of rain triggered enormous mudslides and severe flooding throughout southern Taiwan. One mudslide buried the entire town of Xiaolin killing an estimated 500 people in that village alone. The slow moving storm also caused widespread damage in China, leaving eight people dead and causing $1.4 billion (U.S.) in damages. Nearly 2000 homes were destroyed in the country and 136 000 more were reported to have sustained damage. The storm also caused severe flooding in the northern Philippines that killed 26 people.

[9] Here we consider only one landfall per TC. If a TC makes more than one landfall, the landfall event with the highest wind speed is considered.

The Philippines were severely affected by the 2009 TY season. The PAGASA-named depressions in January, February, and May brought heavy rains and flooding in the eastern Philippines, mudslides on Cebu Island, and heavy rains with flooding in the western Philippines. These were followed by typhoons Kujira and Chan-Hom in May, which caused severe damage to crops, livestock, and infrastructure, as well as deaths in the country. In June, TSs Linfa, Nangka and Soudelor also affected the Philippines. More destruction and deaths were caused by TS Goni in July. In September, the Philippines were again affected by TYs Koppu, Ketsana, and Parma, the second bringing a record rainfall amount in Manila, while the latter made three landfalls in the Philippines. In October, TY Mirinae crossed the Philippines, and in November TD Urduja brought landslides to the southern part of Luzon.

5) Indian Ocean basins

(i) North Indian Ocean (NIO)—M. C. Kruk and K. L.Gleason

The NIO TC season typically extends from April to December, with two peaks in activity during May–June and November when the monsoon trough is positioned over tropical waters in the basin. TCs in the NIO basin normally develop over the Arabian Sea and Bay of Bengal between latitudes 8°N and 15°N. These systems are usually short-lived and relatively weak and often quickly move into the Indian subcontinent. However, strong and "severe cyclonic storms"[10] can develop with winds exceeding 130 kt (Neumann et al. 1993).

The 2009 TC season produced five NSs, one cyclone (CYC), and no major cyclones (MCYC) (Fig. 4.23a). These values are near the 1981–2005 averages of 4.6 NSs, 1.4 CYCs, and 0.5 MCYCs. The season produced an ACE index value of 6.0 x 10^4 kt^2, which is far below the 1981–2005 mean of 16 x 10^4 kt^2 (Fig. 4.23b). There is generally a reduction in tropical cyclone activity, especially in the Bay of Bengal, during the warm phase of ENSO (Singh et al. 2000), which the globe was transitioning to during the boreal summer 2009.

During 2009, the monsoon trough set in relatively early (23 May). However, from 24 to 25 May, CYC Aila developed with peak winds of 65 kt in the Bay of Bengal and disrupted the normal northward advancement of the monsoon. This resulted in severe drought conditions across the typical rainy areas of Jharkhand, Uttar Pradesh, and Himachal Pradesh. However, by 3 July, the monsoonal position had returned to near-normal (Fig. 4.24).

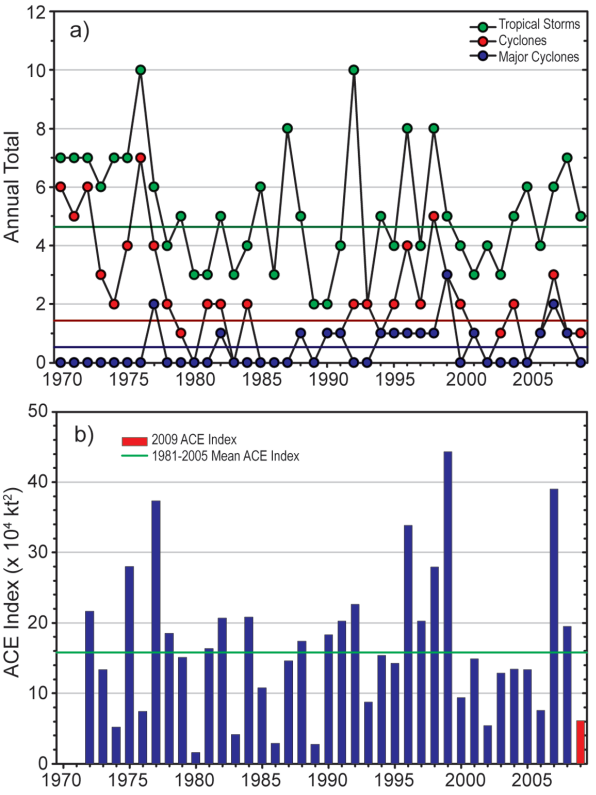

Fig 4.23. Annual TC statistics for the NIO over the period of 1970-2009: (a) number of NSs, CYCs, and MCYCs, and (b) the estimated annual ACE Index (x 10^4 kt^2) for all tropical cyclones during which they were at least tropical storm or greater intensities (Bell et al. 2000). The 1981–2005 base period means are included in both (a) and (b). Note that the ACE Index is estimated due to a lack of consistent 6-hr-sustained winds for every storm.

Despite the below normal rainfall from the monsoon trough, three NSs that made landfall in 2009 ranked among the wettest ever observed in India and Bangladesh. In India, CYC Aila killed 149 people and stranded tens of thousands of others because of the massive flooding that resulted. The eastern state of Meghalaya received 270 mm total rainfall from 25 to 26 May. In Bangladesh, CYC Aila resulted in 179 deaths from flooding and isolated over 400 000 people as numerous villages were submerged from floodwaters. Total rainfall from CYC Aila exceeded 130 mm near Chittagong, Bangladesh. This rainfall was particularly devastating, as it followed on the heels of NS Bijli (14–17 April), which produced an estimated

[10] The Bangladesh Supercyclone of 1970 produced perhaps the greatest human death toll (300 000 persons) on record, primarily from storm surge flooding of low-lying deltas (Holland 1993).

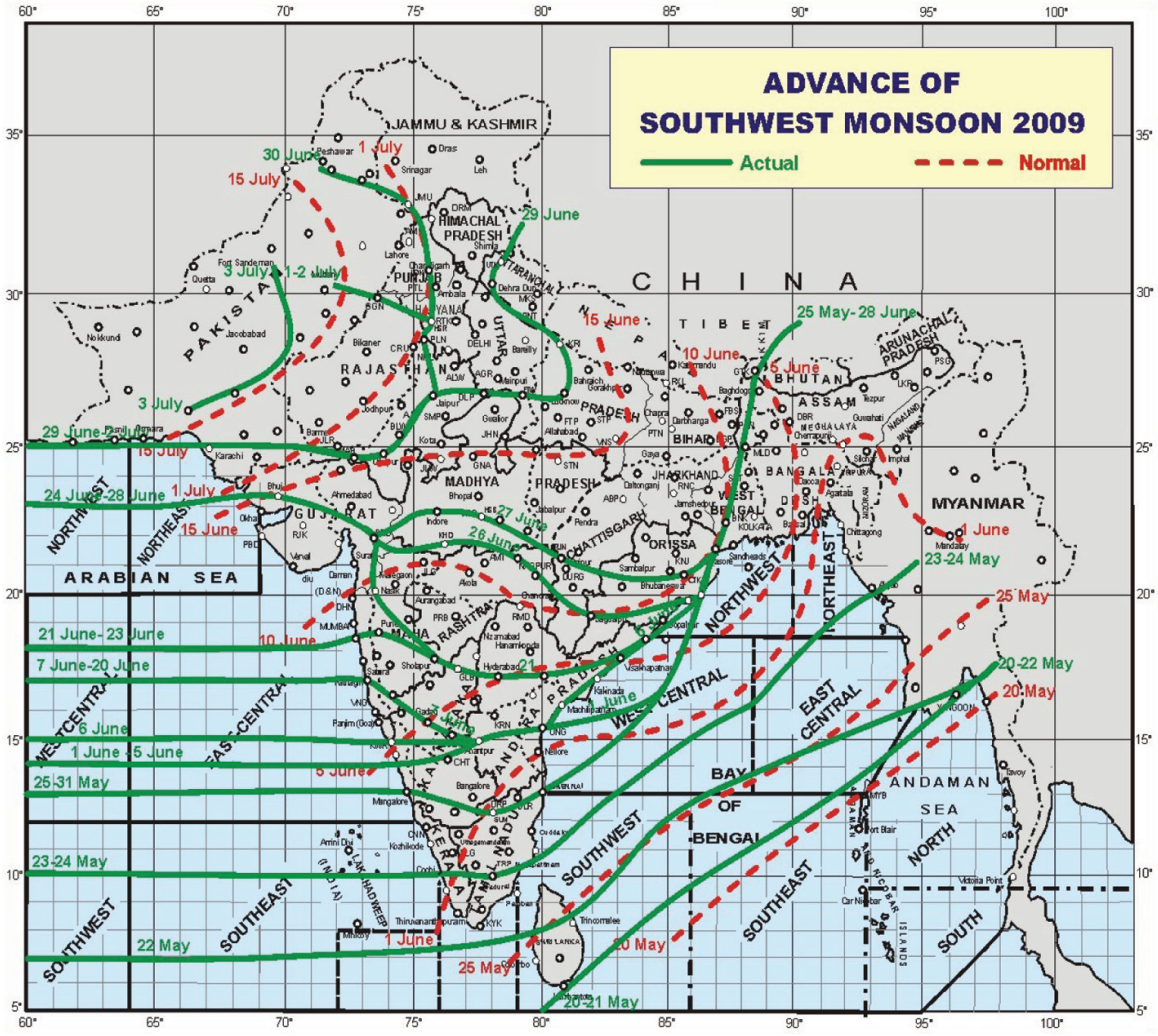

Fig 4.24. The average position of the monsoon trough by date during 2009. (Image source: India Meteorological Department.)

129 mm of rainfall over Bangladesh, according to the Tropical Rainfall Measuring Mission (TRMM), with maximum rainfall rates exceeding 50 mm hr^{-1}.

Finally, from 9 to 11 November, NS Phyan developed just southwest of Sri Lanka and moved steadily north-northwest and then northeast until making landfall along the eastern coast of India near Maharashtra. NS Phyan produced extremely heavy rainfall of 820 mm over Tamil Nadu with peak winds near 50 kt. This total rainfall ranks second only to CYC Nisha, which produced 1000 mm across the same region from 25 to 29 November 2008.

(ii) South Indian Ocean (SIO)—K. L. Gleason and M. C. Kruk

The SIO basin extends south of the equator from the African coastline to 105°E[11], with most CYCs developing south of 10°S. The SIO TC season extends from July to June encompassing equal portions of two calendar years (e.g., the 2009 season is comprised of storms from July to December 2008 and January to June 2009). The peak activity typically occurs from December to April when the ITCZ is located in the Southern Hemisphere and is migrating toward the equator. Historically, the vast majority of the landfalling CYCs in the SIO impact Madagascar, Mozambique, and the Mascarene Islands, including Mauritius and Réunion.

[11]In order to generate consistent basin statistics, the SIO basin boundary overlaps with the Australian Bureau of Meteorology's operational warning area from 90°E to 105°E.

The historical SIO TC data is probably the least reliable of all the TC basins (Atkinson 1971; Neumann et al. 1993), primarily due to a lack of historical record keeping by individual countries and no centralized monitoring agency; however, the historical dataset for the region has been updated (Knapp et al. 2010). The historical data are noticeably deficient before reliable satellite data were operationally implemented in the region beginning about 1983.

The 2008/09 season produced 13 NSs and near-average numbers of CYCs (5) and MCYCs (3) (Fig. 4.25a). The 1981/2005 averages are 11.8 NSs, 6.4 CYCs, and 3 MCYCs. However, the 2008/09 ACE index (~70 x 10^4 kt^2) was below the 1981/2005 average (Fig. 4.25b). With the exception of the 2001–02 season, no other season since the mid-1990s has produced an above average seasonal ACE in the SIO basin.

The strongest CY during the season was MCYC Gael, which developed in the central Indian Ocean during the first few days of February 2009. As it moved southwestward, the center of circulation remained north of the Mauritius and Reunion Islands and slowly became more organized amidst the warm SSTs and weak upper-level wind shear and was declared a tropical cyclone on 3 February by JTWC. Gael quickly intensified just north and west of Reunion and became a MCYC on 6 February. Gael began to curve to the south and then east, missing a direct strike to Madagascar, and the storm remained at sea as it continued along a southeasterly direction and eventually dissipated. MCYC Gael reached peak strength of 120 kt and was responsible for two fatalities on Reunion Island.

The strongest landfalling storm of the season formed in the Mozambique Channel in mid-January 2009 and remained quasi-stationary as it became better organized. By 18 January, Fanele became a tropical cyclone and intensified rapidly into a MCYC on 20 January with sustained winds of 100 kt. MCYC Fanele made landfall on the west coast of Madagascar on 21 January in the Menabe Region southwest of Morondava. Weakened severely by the interaction with the land, Fanele entered the Indian Ocean as a tropical depression and regained some strength before becoming extratropical. At least eight fatalities were reported as a result of MYC Fanele. Fanele's landfall occurred just two days after TS Eric brushed the eastern coast of Madagascar. The two CYCs impacted more than 50 000 people and left thousands homeless.

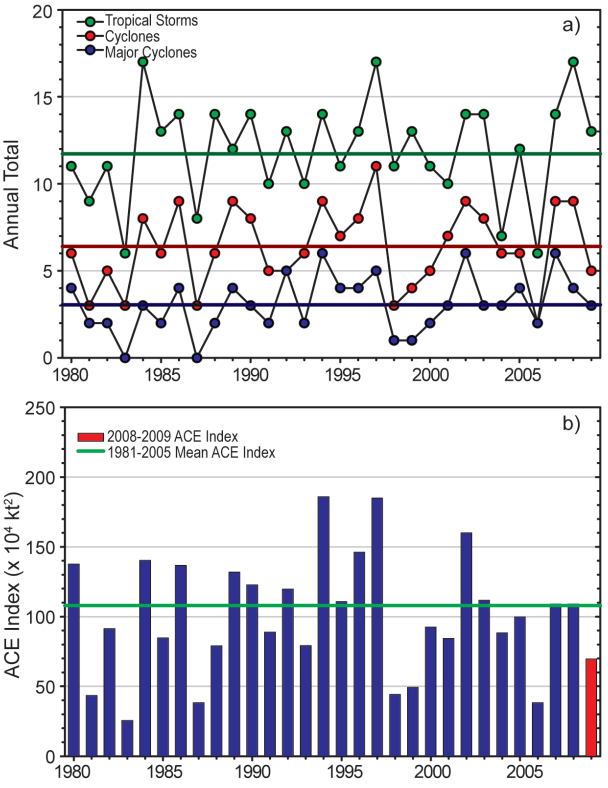

Fig. 4.25. Annual TC statistics, with long-term mean, for the SIO over the period of 1970–2009: (a) number of NSs, CYCs, and MCYCs, and (b) the estimated annual ACE Index (x 10^4 kt^2) for all tropical cyclones during which they were at least tropical storm or greater intensities (Bell et al. 2000). The 1981–2005 base period means are included in both (a) and (b). Note that the ACE Index is estimated due to a lack of consistent 6-hr-sustained winds for every storm.

6) Southwest Pacific basin—A. M. Lorrey, S. McGree, and J. Renwick

Eight TCs occurred in the Southwest Pacific during the 2008/09 season, which was one less than the long-term average (1969/70 to 2007/08). This was the most active TC season for the region since 2005/06. The first TC formed on 28 January, which was the latest start to the Southwest Pacific TC season since 2000/01. Four systems developed into TCs west of the international date line and four TCs formed east of it. Peak activity occurred in March (four TCs), and December and February were unusually quiet. Only one TC reached hurricane intensity (sustained wind speeds of at least 64 kt). TC Hettie was the first to form in the southwest Pacific during the 2008/09 season and developed on 28 January to the southeast of Fiji. This system brought southerly winds and heavy rain to the central district of Fiji on 28–29 January before dissipating on 30 January.

Early on 30 January, a tropical low formed in the Coral Sea region and intensified into TC Ellie, a Cat- 1 storm, on 1 February. TC Ellie reached peak winds of 43 kt and made landfall in Australia on 2 February. Torrential rain from the dying end of this storm flooded parts of Northern Queensland and caused damages estimated at $110 million (AUS). TC Innes was the third to form in the southwest Pacific and initiated on 13 February as a tropical depression east of Fiji. On 17 February, after passing over Vanuatu and moving toward New Caledonia, Innes was upgraded to a TC. No significant impacts or loss of life were reported from this system. Subsequently, on ex-tropical transition, the dying remains of TC Innes merged with a low pressure system to the east of Australia that generated significant rainfall in northern New Zealand.

Four TCs affected the southwest Pacific region during March. TC Hamish formed off the Australian coast in the Coral Sea on 5 March. TC Joni followed on 11 March, and formed near the Southern Cook Islands and attained a maximum intensity of 55 kt. Damage in the Southern Cooks from TC Joni was minimal. TC Ken then formed between Niue and the Southern Cook Islands on 17 March, attained a maximum intensity of 50 kt, and did not affect land areas. TC Jasper entered the southwest Pacific from the Coral Sea on 24 March with storm intensity and later passed through New Caledonia's waters, with no significant damage reported. Only one TC (Lin) formed in the basin during April. TC Lin formed on 4 April east of Fiji and passed over Tongatapu on 5 April. Sustained winds for Lin were estimated at 55 kt with gusts up to 80 kt closer to the storm's center.

7) Australian Region basin—B. C. Trewin

The 2008/09 TC season was near normal in the broader Australian basin (areas south of the Equator and between 90°E and 160°E[12], which includes Australian, Papua New Guinea, and Indonesian areas of responsibility). The season produced 10 TCs, equal to the long-term average. There were four TCs in the eastern sector[13] of the Australian region during 2008/09, five TCs in the western sector (one of which formed in the northern sector before moving west), and one in the northern sector. There were four landfalls during the season.

The most intense TC of the season was Hamish, which tracked south-east, parallel to the Queensland coast, from 5 to 11 March. It reached its maximum intensity on 7 March while near 19°S, 150°E (approximately 200 km offshore from Bowen), with estimated maximum gusts of 160 kt, maximum sustained winds of 115 kt, and a minimum central pressure of 925 hPa, making it the most intense cyclone observed[14] in the vicinity of the Queensland coast since 1918. It remained at Cat- 4 or 5 intensity[15] for three days. While Hamish posed a substantial potential threat to the Queensland coast, it did not make landfall or approach the coast closely enough to cause any significant damage on land. However, two lives were lost at sea, and damage to a ship from the associated large waves resulted in a serious oil slick and coastal pollution in the Brisbane area.

Four TCs made landfall during the season, the strongest being Cat- 2. None caused significant damage through wind or storm surge, but all were associated with flooding. Billy made landfall near Wyndham, Western Australia on 20 December as a Cat- 2 system, causing minor tree damage and widespread flooding through the Kimberley region. The system later reintensified as it moved back over the ocean and ultimately peaked at Cat- 4 intensity (maximum gusts 135 kt, maximum sustained winds 95 kt, minimum central pressure 950 hPa) on 24 December, when north of Port Hedland and moving away from the coast.

Two short-lived Cat- 1 systems affected Queensland early in 2009. Charlotte made landfall near the Gilbert River Mouth, on the east coast of the Gulf of Carpentaria, on 12 January, while Ellie made landfall north of Cardwell, on the east coast, on 1 February. Both moved over areas that were already experiencing flooding and hence exacerbated conditions. The Herbert River catchment was severely affected, particularly around Ingham, which received 1481 mm of rain from 25 January to 9 February, including 949 mm from 30 January to 4 February. The heaviest daily total associated with the system was 497 mm at Hawkins Creek, northwest of Ingham.

[12]The Australian Bureau of Meteorology's warning area overlaps both the southern Indian Ocean and Southwest Pacific.

[13] The western sector covers areas between 90°E and 125°E. The eastern sector covers areas east of the eastern Australian coast to 160°E, as well as the eastern half of the Gulf of Carpentaria. The northern sector covers areas from 125°E to the western half of the Gulf of Carpentaria.

[14] Note that it is likely that the intensity of many cyclones was underestimated prior to the use of satellite data from the 1970s.

[15]See http://www.bom.gov.au/weather/cyclone/faq/index.shtml for a definition of Australian TC categories.

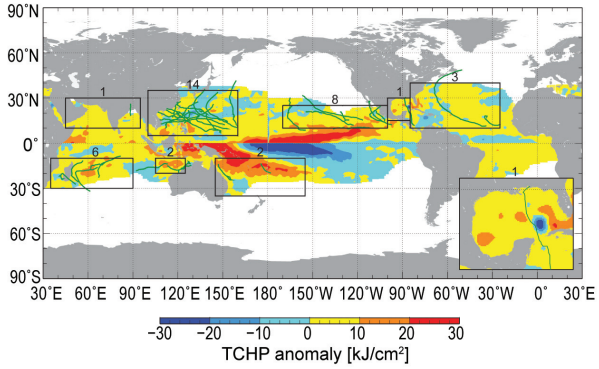

Fig. 4.26. Global anomalies of TCHP corresponding to 2009 computed as described in the text. The boxes indicate the seven regions where TCs occur: from left to right, Southwest Indian, North Indian, West Pacific, Southeast Indian, South Pacific, East Pacific, and North Atlantic (shown as Gulf of Mexico and tropical Atlantic separately). The green lines indicate the trajectories of all tropical cyclones reaching at least Cat- 1 (1-minute average maximum wind ≥119 km hr^{-1}) and above during November 2008–December 2009 in the Southern Hemisphere and 2009 in the Northern Hemisphere. The numbers above each box correspond to the number of Cat- 1 and above cyclones that travel within each box. The Gulf of Mexico conditions during June–November 2009 are shown in detail in the insert shown in the lower right corner.

The fourth landfalling system of the season was Dominic, a Cat- 2 system (maximum gusts 75 kt, maximum sustained winds 55 kt, minimum central pressure 976 hPa) which made landfall near Onslow, Western Australia on 27 January. As for the Queensland systems, the principal impact was flooding, with daily rainfall totals of 243 mm at Thevenard Island and 238 mm at Onslow Airport. Of those TCs that did not make landfall, the most intense was Ilsa, which peaked at Cat- 3 intensity (maximum gusts 125 kt, maximum sustained winds 90 kt, minimum central pressure 958 hPa) on 19 March when more than 1000 km off the Western Australian coast, near 16°S, 107°E.

e. *TC heat potential (TCHP)*—G. J. Goni, J. A. Knaff, and I-I Lin

TCHP is discussed here for the seven TC basins previously documented as a way to summarize that activity from a slightly different perspective. The TCHP, defined here as the ocean heat content contained between the sea surface and the depth of the 26°C isotherm, has been shown to be more closely linked than SST to intensity changes (Shay et al. 2000; Goni and Trinanes, 2003; Lin et al., 2008, 2009), provided that atmospheric conditions are also favorable. The TCHP shows high spatial and temporal variability associated with oceanic mesoscale features that can be globally detected with satellite altimetry TCHP (Goni et al. 2009). In general, the real-time forecast of TC intensity is highly dependent on track forecasts and many of the errors introduced in the track forecast are translated into the intensity forecast (Mainelli, et al. 2008). Clearly, areas with high values of TCHP may be important only when TCs travel over them.

To examine the interannual variability of TCHP with respect to TCs, TCHP anomalies are computed during the months of TC activity in each hemisphere: June through November 2009 in the Northern Hemisphere and from November 2008 through April 2009 in the Southern Hemisphere. Anomalies are defined as departures from the mean TCHP calculated during the same months for the period 1993 to 2009. These anomalies show large variability within and among the TC basins (Fig. 4.26).

The WNP basin exhibits the anomalies from the El Niño conditions, which have been in place in the equatorial Pacific Ocean since June 2009. Similar to the conditions during 2008, the South Pacific basin showed mostly positive anomalies. The NIO basin exhibited positive values in the Bay of Bengal and in the Arabian Sea. The Gulf of Mexico (Figs. 4.26, 4.27) showed mostly positive values except for a small region of negative values, which was probably due to a different location of the Loop Current. The tropical Atlantic exhibited mostly positive values, which is also observed in sea height and SST fields (http://www.aoml.noaa.gov/phod/regsatprod/atln/index.php).

The ENP season was very active although the first named storm of the season did not develop until late in June, being the latest start of the ENP

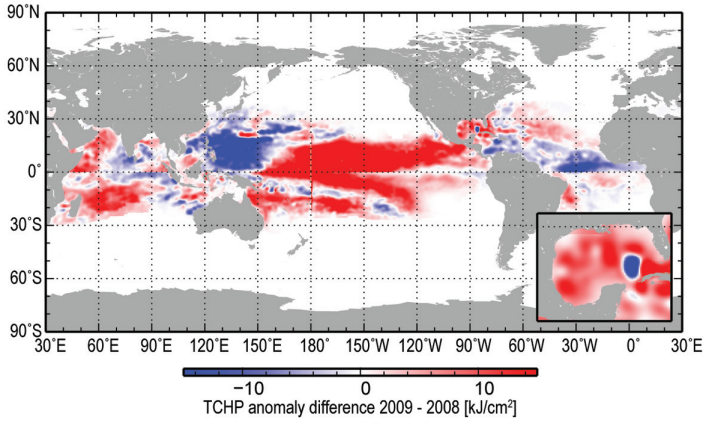

Fig. 4.27. Differences between the TCHP fields in 2009 and 2008.

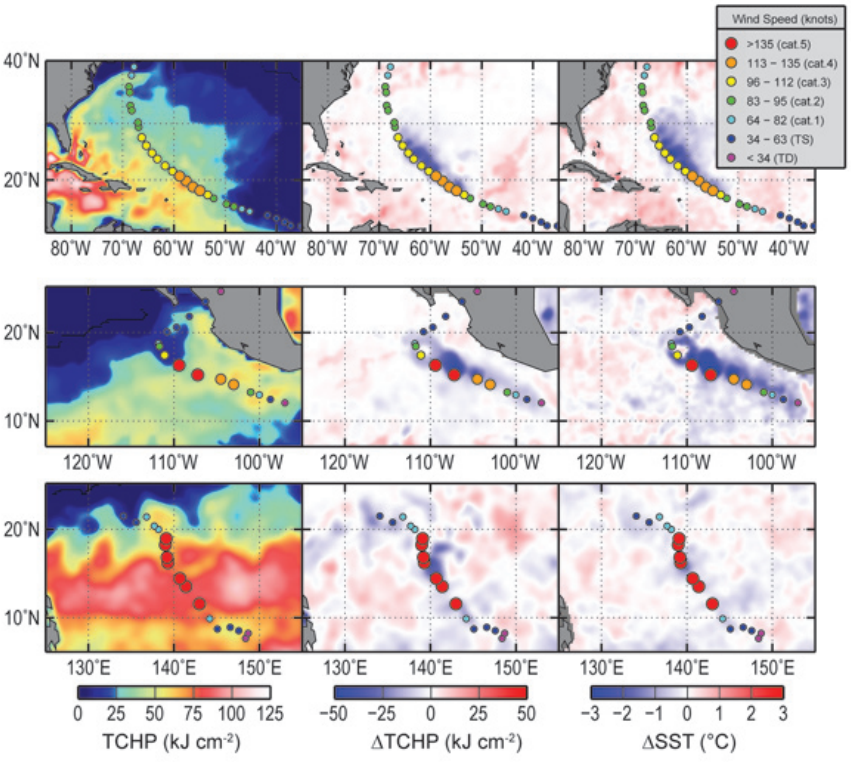

Fig. 4.28. (Left) TCHP, and surface cooling given by the difference between post- and pre-storm values of (center) tropical cyclone heat potential and (right) sea surface temperature, for (from top to bottom) Hs Bill and Rick, and TY Nida.

hurricane season in 40 years. H Rick reached Cat-5 in mid-October, and became the first Cat-5 ENP H since Kenna in 2002 and the second strongest ENP hurricane on record, behind Linda in 1997. H Rick intensified from Cat- 2 (85 kt, 975 hPa) to Cat- 5 (150 kt, 914 hPa) in one day. Six hours later Rick reached a maximum intensity of 155 kt just off the southern coast of Mexico (Fig. 4.28). This rapid rate of intensification occurred while traveling over a region of very high TCHP (above 70 kJ cm^{-2}) and in a favorable atmospheric environment. This TC weakened as quickly as it intensified under the influence of strong upper-level southwesterly wind associated with an amplified short-wave trough (Cangialosi and Avila 2010).

The WNP TY season was calmer than average in the early part of the season (June–August) but became very active during the later part of the season (September to November). During these three months, five Cat- 4 and 5 TYs developed, as compared to two in 2008. This happened despite the general cooling tendency of TCHP due to El Niño (Figs. 4.26 and 4.27) in the western Pacific in 2009. Although the TCHP in the western Pacific decreased by about 10–15 kJ cm^{-2} with respect to the average conditions and to 2008 (Figs. 4.26 and 4.27), this was only a small decrease compared to typical TCHP values (Lin et al. 2008). In the WNP, especially between the 10°N and 20°N latitudinal belt, the TCHP values are typically around 100–160 kJ cm^{-2} (Lin et al. 2008). Therefore, even with a 10–15 kJ cm^{-2} decrease, the resultant TCHP in 2009 was still around 85–140 kJ cm^{-2} (Lin et al. 2008), sufficient to keep the TY's self-induced ocean cooling negative feedback small during the intensification (Lin et al. 2009).

TY Nida was a Cat- 1 storm on 24 November and intensified into a Cat- 5 STY on 25 November, reaching peak winds of 160 kt, according to the preliminary JTWC best tracks. The track of this TY travelled from a region of high (~50 kJ cm^{-2}) TCHP values to over a region of extremely high (above 100 kJ cm^{-2}) values. The strength of this TY is also independently revealed by its large 10-minute sustained winds of 115 kt estimated at the same time in the final best track produced by RSMC Tokyo, the greatest intensity since TY Jangmi in 2008. However, the cooling produced by this TY was only of approximately 1°C, probably because of the very deep warm and stable surface layer (Fig. 4.28).

f. Intertropical Convergence Zones (ITCZ)

1) Pacific—A. B. Mullan

There are two prominent convergence zones in the Pacific: the ITCZ in the Northern Hemisphere, lying approximately parallel to the Equator with a slight poleward tilt on its eastern end and varying in position from around 5°N–7°N in February–May to 7°N–10°N in August–November; and the SPCZ, which extends diagonally from around the Solomon Islands (10°S, 160°E) to near 30°S, 140°W and is most active in the November–April half-year. A southern branch of the ITCZ can also occur but is only apparent in the January–May period and is strongest in La Niña years.

Figure 4.29 shows 20°N to 30°S transects of quarterly rainfall in the Pacific, as derived from the 0.25

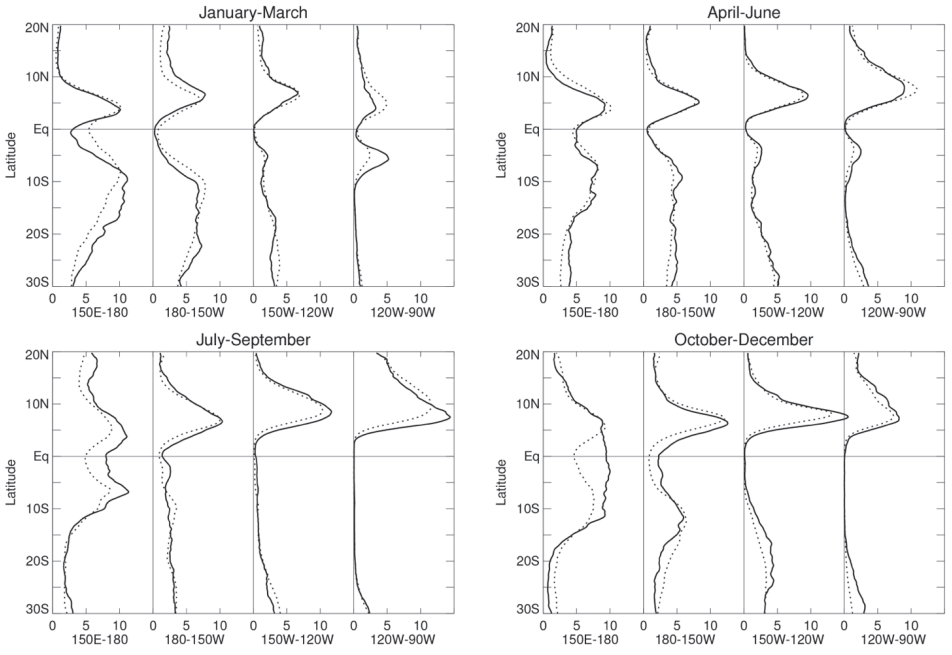

Fig. 4.29. Rainfall rate (mm/day) from TRMM 0.25 degree analysis for the four quarters of 2009. The separate panels for each quarter show the 2009 rainfall cross-section between 20°N and 30°S (solid line) and the 1999–2008 climatology (dotted line), separately for four 30° sectors from 150°E–180° to 120°W–90°W.

degree resolution NASA TRMM rainfall data (3B-43 product, Huffman et al. 2007). The convergence zones are clearly evident in the transects over progressive 30-degree longitude bands across the Pacific, where the 2009 positions can be compared with the short 10-year climatology 1999–2008. TRMM data are also available for 1998; this year was omitted from the climatology due to the extremely unusual position of the convection on that year, although in fact the only noticeable effect of including 1998 would be to increase the rainfall along the equator east of the international date line during the first quarter of the year.

La Niña conditions strengthened at the end of 2008, and during the first quarter of 2009 the convergence zones reflected typical La Niña characteristics, with the ITCZ and SPCZ both poleward of their climatological positions and suppressed convection evident near the international date line (Fig. 4.29 and the top panel of Fig. 4.30). Many islands of the southwest Pacific (Vanuatu, New Caledonia, Fiji, Tonga, Samoa, and Southern Cooks) experienced above normal rainfall during this season, with January being particularly wet in Fiji where many new rainfall records were set (ICU 2009). In February, the southern ITCZ appeared and remained prominent for the following two months until ENSO-neutral conditions were established.

ENSO-neutral conditions continued through much of the second quarter of 2009, with the Pacific convergence zones mostly near their normal position and intensity. During this season, the SPCZ tends to contract so that by June only the far western end near Papua New Guinea is active; conversely, the ITCZ strengthens on its eastern end from 150°W eastward. In the western Pacific (150°E–180°), the ITCZ was weaker on its northern edge and resulted in persistent very dry conditions in the northern atolls of the Marshall Islands (PEAC 2009; Fig. 4.29 top right panel).

El Niño conditions had established themselves by July but were initially weak. During the second half of 2009, the ITCZ east of the Dateline tended to be

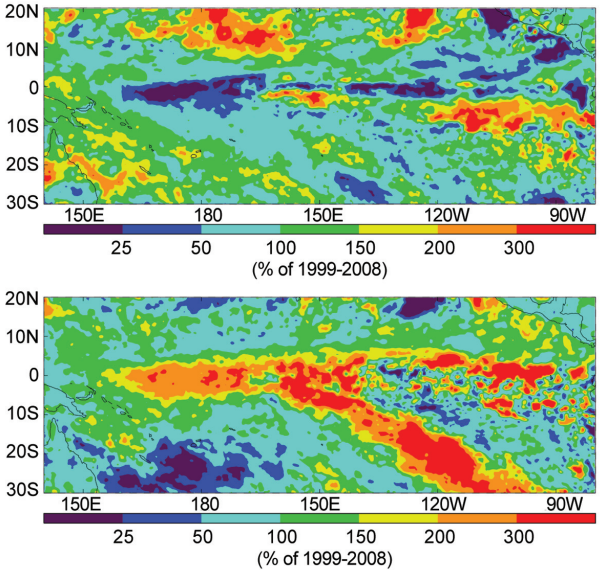

Fig. 4.30. Average rainfall rate from TRMM 0.25 degree analysis for January–March 2009 (top) and October–December 2010 (bottom), as a percentage of the 1999–2008 climatology.

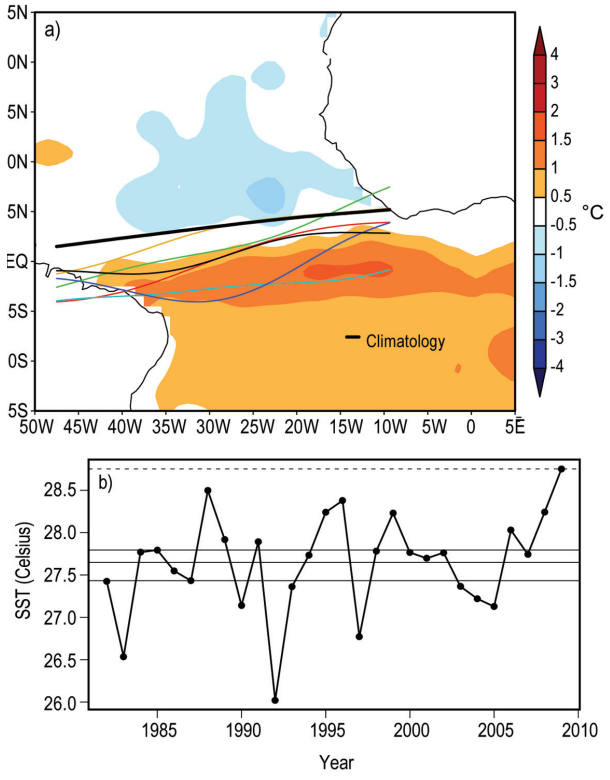

Fig. 4.31. (a) Atlantic ITCZ position inferred from outgoing longwave radiation during May 2009. The colored thin lines indicate the approximate position for the six pentads of May 2009. The black thick line indicates the Atlantic ITCZ climatological position. The SST anomalies (Reynolds et al. 2002) for May 2009 based on the 1982-2009 climatology are shaded. (b) SST time series averaged over the Atlantic warm pool (5°W to 30°W, 0°S to 5°S) for the period 1982–2009. The solid horizontal central line indicates the climatological mean. The other solid horizontal lines represent the upper and lower terciles. The dashed horizontal line puts the May 2009 record value in climate perspective.

equatorward of its normal position and often more intense (Fig. 4.29). In the OND quarter the SPCZ typically reintensifies, but this year the SPCZ was weak, with suppressed convection in the central portion of the southwest Pacific. Rainfall in the islands was very variable, but a number of islands (New Caledonia, Vanuatu, Fiji, Tonga, and French Polynesia) experienced some months of very low rainfall during this period. By contrast, enhanced convection occurred along the Equator west of the Dateline (Western Kiribati). Fig. 4.30 summarizes this typical El Niño rainfall pattern; the increased rainfall along a line from 5°S, 150°W to 20°S, 120°W appears very significant, but this band of stronger convection is at the very northeast edge of the SPCZ and the rainfall amounts are not very large.

For 2009 as a whole, the TRMM data suggests rainfall was between 50% and 150% of normal over most of the equatorial and tropical Pacific (except in the far eastern sector south of the Equator), reflecting the influence of opposite ENSO phases during the year.

2) Atlantic—A. B. Pezza and C. A. S. Coelho

(i)Description

The Atlantic ITCZ is a well-organized convective band that oscillates approximately between 5°N–12°N during July–November and 5°N–5°S during January–May (Waliser and Gautier 1993; Nobre and Shukla 1996). As equatorial Kelvin waves can modulate its interannual variability, ENSO is also known to influence it on a seasonal scale (Münnich and Neelin 2005). In 2009, the Atlantic ITCZ was influenced by ENSO and the Atlantic SST gradient between the Northern and the Southern Hemisphere. A transition occurred from a weak La Niña (January–March) to El Niño towards the end of the year, but the dynamic signature in the Atlantic was also very marked with a strong SST gradient towards the Southern Hemisphere during the first half of the year (warmer towards the south, Fig. 4.31a) changing into a reversed gradient pattern in the second half. As a result the ITCZ reached its southernmost position and maximum intensification in April and May, rapidly migrating back to the north from mid-June. The maximum intensification in May was accompanied by outbursts of severe convection facilitated by the ITCZ migrating into the core of the 'Atlantic warm pool' with SSTs of the order of 30°C (Fig. 4.31b) and high values of CAPE producing positive rainfall anomalies over a large area of northeastern South America and adjacent ocean near the equator (Fig. 4.32a and b).

(ii) Air France 447 disaster: did the Atlantic warm pool play a role?

These formations are not rare but are within the variability of an enhanced pattern intrinsic to years of very active ITCZ. It was unfortunate that a routine commercial flight between Rio de Janeiro and Paris starting its trip on the evening of 31 May (Brazilian time) crossed overnight an area of strong cumulus towers (cold tops) under development at about 3°N (Fig. 4.33), crashing into the ocean at about 0200 UTC on 1 June. The accident made headlines internationally and raised the question as to whether it is safe to fly over the ITCZ during very active periods. We note that there is no definite proof of causality

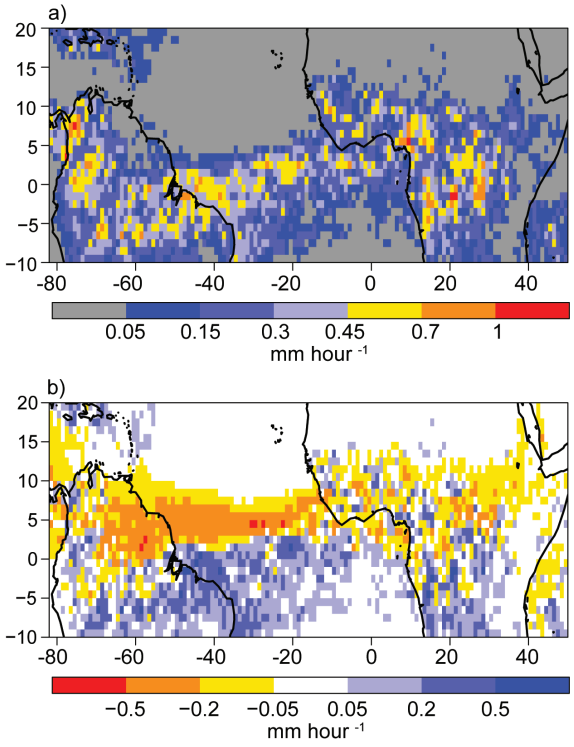

Fig. 4.32. TRMM (a) mean and (b) anomalous precipitation rate (mm hr^{-1}) for May 2009. The anomaly was based on the climatology for the period 1982–2008.

between the behavior of the ITCZ and the plane crash, but evidence suggests that the weather was an influencing factor. The enhancement observed in May 2009 was a partial thermodynamic response to the large warm pool directly underneath the ITCZ coupled with the dynamic synergy of an already low static stability in the large scale due to the suppressed Kelvin wave propagation from the Pacific during a southern summer of weak La Niña, which would have established anticyclonic conditions over the area. The SST averaged over the Atlantic warm pool in May was the highest on record for the period from 1982 to 2009, suggesting a connection with the unusual enhancement observed (Fig. 4.31b).

g. Indian Ocean Dipole (IOD)—J. J. Luo

The IOD is an internal air-sea coupled climate mode in the tropical Indian Ocean (IO). It can be driven by the tropical Pacific ENSO or sometimes occur independently (Luo et al. 2008, 2010). Positive IOD features anomalous SST cooling in the eastern IO and weak warming in the west during boreal summer and fall and vice versa for negative IOD. Associated with its strong nonlinearity, positive IOD is usually more intensive and predictable than negative

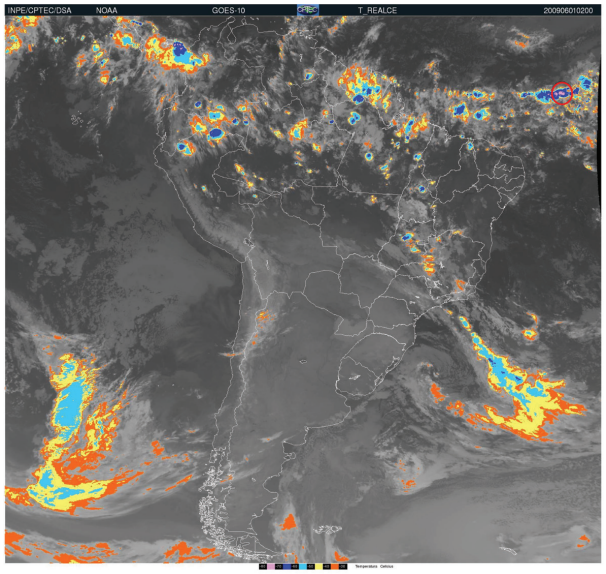

Fig. 4.33. NOAA GOES-10 infrared satellite photo with enhanced color scheme depicting the approximate time of the crash of Air France flight 447 from Rio de Janeiro to Paris on the morning of 1 June. The red circle near the equator indicates the likely position where the crash occurred.

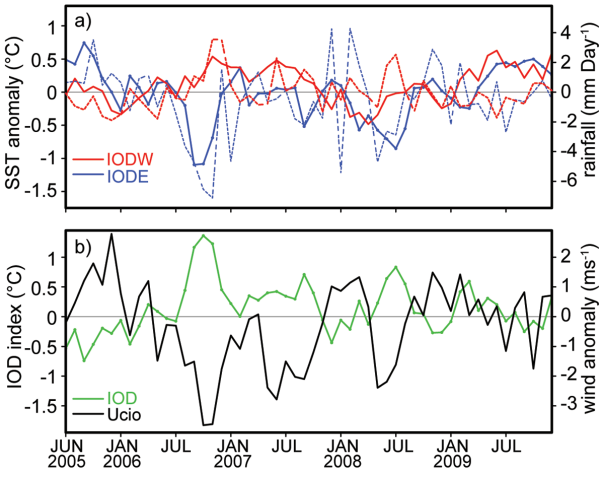

Fig. 4.34. (a) Monthly anomalies of SST (°C, solid lines) and precipitation (mm day^{-1}), dashed lines) in the eastern (IODE, 90E°–110°E, 10°S–0°, blue lines) and western pole (IODW, 50°E–70°E, 10°S–10°N, red lines) of IOD. (b) As in (a), but for the IOD index (measured by the SST difference between IODW and IODE) and surface zonal wind anomaly (m s^{-1}) in the central equatorial IO (70°E–90°E, 5°S–5°N). The anomalies were calculated relative to the climatology over the period 1982–2008. These are based on the NCEP optimum interpolation SST (www.emc.ncep.noaa.gov/research/cmb/sst_analysis/), NCEP CPC CAMS_OPI precipitation (http://iridl.ideo.columbia.edu), and NCEP atmospheric reanalysis data.

IOD. Following the three unprecedented consecutive positive IODs during 2006–08, SST anomalies in the tropical IO during June to November 2009 reflected a neutral-to-weak negative IOD condition (Fig. 4.34). SSTs in the eastern and western tropical IO were warmer than normal since April–May 2009, presumably due to more solar radiation reaching the sea surface associated with the dry conditions there (Fig. 4.34a). The nearly in-phase relationship between SST and rainfall anomalies in the western and eastern poles of IOD during 2005–08 was broken in 2009; SST anomalies in the two poles during 2009 appear to be driven by the atmosphere rather than a forcing of the convection anomalies. Correspondingly, zonal surface wind anomalies in the central equatorial IO showed no or less relationship with the west–east SST gradient during 2009 (Fig. 4.34b). In contrast to the pronounced low-frequent variations and well-coupled conditions during 2005–08, the wind anomalies in 2009 were characterized by high-frequency fluctuations in response to active intraseasonal oscillations despite a tendency of strengthening easterly anomalies associated with the evolution of La Niña to El Niño in the Pacific. By adjusting the equatorial Walker circulation, ENSO evolution may largely influence the tropical IO climate, particularly in cases when the IO internal air-sea coupled processes are weak. The 2008/09 La Niña event caused more rainfall over the equatorial eastern IO and Maritime Continent during DJF; this cooled the local SSTs and induced westerly wind anomalies in the central-eastern equatorial IO (Fig. 4.35a). The westerly winds drove down-welling equatorial Kelvin waves and deepened the oceanic thermocline in the eastern IO and along the west coast of Sumatra-Java (Fig. 4.36a). An IO basin-wide cooling condition, frequently observed several months after La Niña peak, was however, not well developed in early 2009 (Figs. 4.35a and 4.35b). Warmer SSTs occupied the southwestern IO, northeastern Arabian Sea and Bay of Bengal; this appears to be associated with deeper-than-normal thermocline in these areas (Figs. 4.36a and 4.36b).

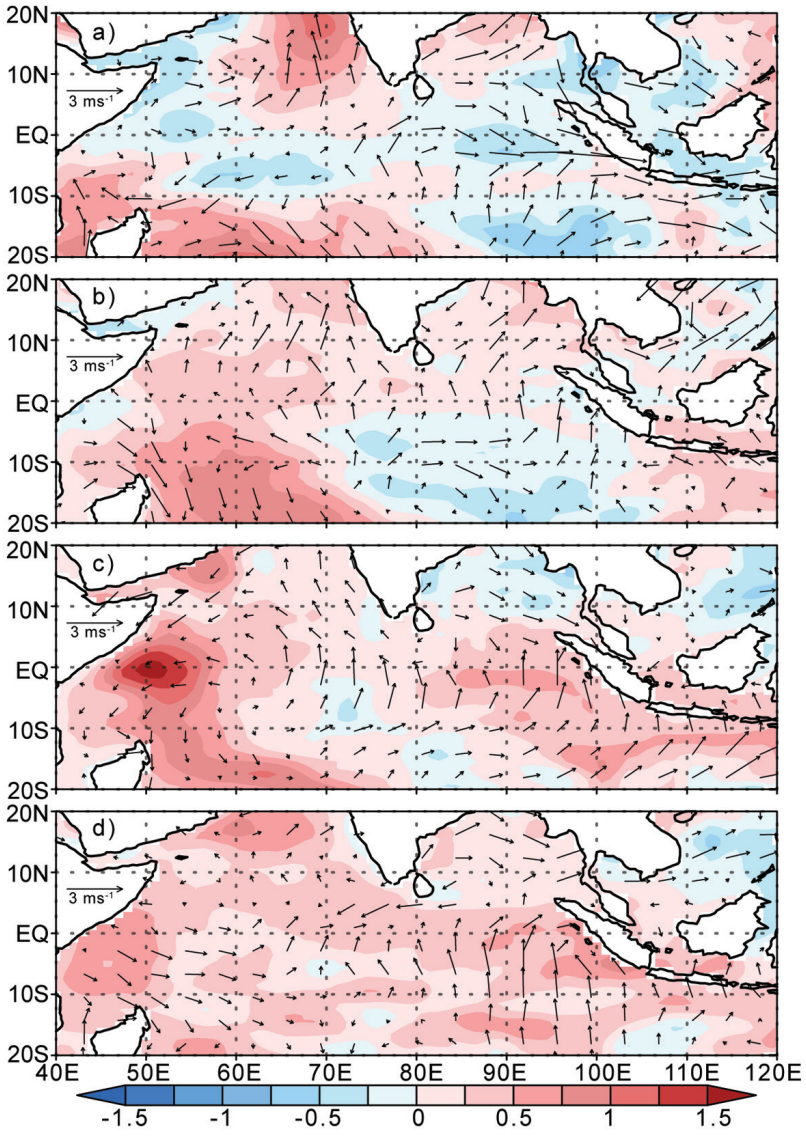

Fig. 4.35. SST and surface wind anomalies during (a) Dec–Feb 2008–09, (b) Mar–May 2009, (c) Jun–Aug 2009, and d) Sep–Nov 2009.

During March–May, warmer SST anomalies started to develop in the western equatorial IO owing to less cloud condition there (Fig. 4.35b). This is related to the La Niña influence and completely decoupled from the local cold subsurface signal (Fig. 4.36b). The cold subsurface signal in the western IO during December 2008 to May 2009 reflected as eastward-propagating equatorial upwelling Kelvin waves and raised the thermocline in the eastern IO (Fig. 4.36c). Meanwhile, the original warm subsurface signal in the

eastern IO reflected as a pair of westward-propagating downwelling Rossby waves and reached the west during JJA; this contributed to the rapid enhancement of the surface warming in the western equatorial IO (Fig. 4.35c). An off-equatorial warm Rossby wave at 10°S also propagated slowly westward from ~73°E to ~53°E during the period from December 2008 to November 2009 (Fig. 4.36). However, it appears to have had little contribution to the western IO SST warming from March to November. Forced by more solar radiation associated with the less cloud condition, SSTs in the eastern IO became warmer than normal during June–August despite the local cold subsurface signal (Figs. 4.35c and 4.36c). The warmer SSTs generated a local wind convergence and deepened the thermocline in the eastern IO which in turn helped to intensify the surface warming (Figs. 4.35d and 4.36d). This led to a weak negative IOD index during September–November, in contrast to what has been often observed during El Niño developing years. The weak negative IOD condition may have caused more rainfall in the eastern IO and Maritime Continent and reduced the short rains in eastern Africa during the boreal fall season, which is counter to the remote influence of the developing El Niño. It is also possible that the eastern IO SST warming might have hampered the El Niño development during 2009 (Luo et al. 2010).

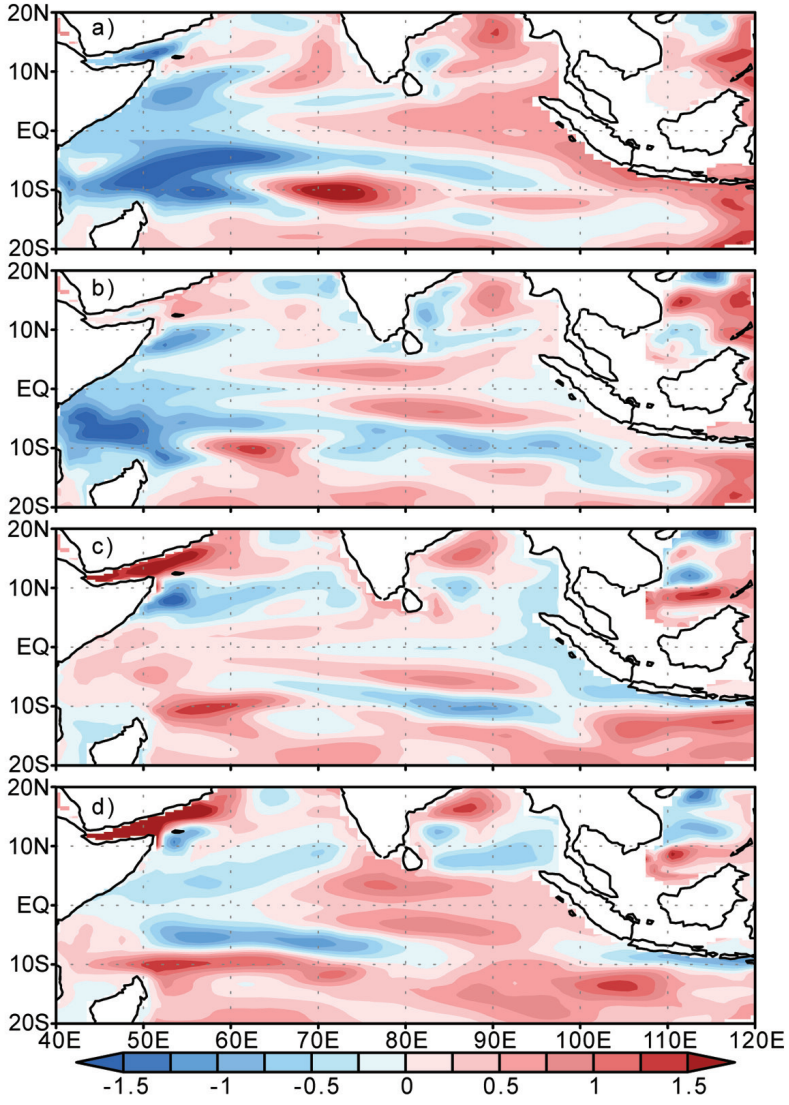

Fig. 4.36. As in Fig. 4.35, but for the upper 300-m mean ocean temperature anomalies based on the NCEP ocean reanalysis (available at www.cpc.ncep.noaa.gov/products/GODAS/).

THE FORGOTTEN SUB-BASIN—THE CENTRAL NORTH PACIFIC (CNP) REEMERGES WITH A FURY IN 2009—D. H. LEVINSON

The CNP, between 140°W and the international date line, is best described as a "sub-basin" of the ENP; no other analog exists in the other global TC basins. On average the CNP experiences four to five TCs per season (Blake et al. 2009). These are typically systems that have propagated westward from the ENP basin where they originally developed in the monsoon trough west of Mexico and Central America. However, every few years the CNP becomes more active for tropical cyclogenesis and storm formation occurs in situ within the sub-basin, well outside of the Main Development Region of the ENP. Therefore, the CNP is an unusual and transient region of TC activity, where the atmospheric and oceanic conditions can be termed "enhanced" or "quiescent" based on large-scale synoptic patterns typically associated with the ENSO phase (Chu and Wang 1997; Chu and Clark 1999; Chu 2002). The 2009 TC season was one such year when the CNP was in an enhanced phase, as seven TCs were officially tracked by NOAA's CPHC, with four of these systems developing within the sub-basin.

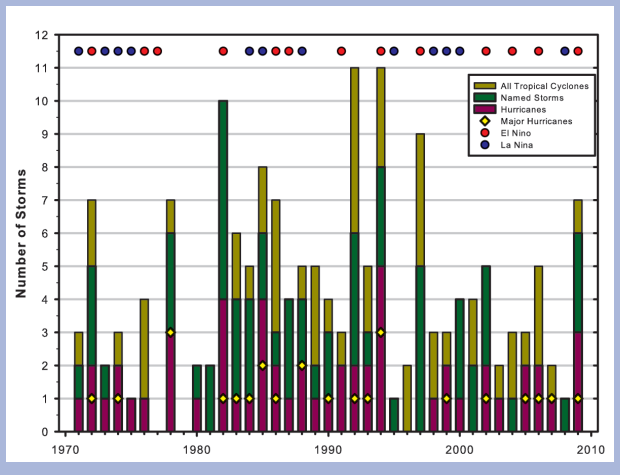

Fig. 4.37. Annual TC activity in the CNP, 1971–2009, with seasonal totals of: TCs including TDs (brown), NSs (green), Hs (purple), and MHs (yellow diamonds). Circles at top denote the ENSO phase (El Niño: red, La Niña: blue) for each TC season.

The rarity of TC activity in the CNP has been known for a long time (e.g., Wann 1974; Chu and Wang 1997; Chu and Clark 1999), but improved monitoring due to satellite coverage since the late 1960s has allowed for a more complete picture of the historical variations of activity in the sub-basin. Figure 4.37 shows the time series of TC activity in the CNP in terms of all TC types (including TDs) since 1971. It is clear from Fig. 4.37 that the sub-basin experiences pronounced interannual and interdecadal variability in the frequency of TC occurrences. Also plotted in Fig. 4.37 are the ENSO phases during July–October when the majority of TC activity occurs in the CNP. Since 1971, most of the enhanced TC seasons have occurred in conjunction with El Niño warm events, although there have been several notable exceptions, such as in 1978, 1985, and 1992.

The CNP sub-basin also exhibits longer-term, multidecadal periods of enhanced and diminished TC activity similar to the ENP basin as a whole (and inverse to the North Atlantic; Wang and Lee 2010). Previous studies identified epochs of lower activity and higher activity associated with changes in the large-scale atmospheric and oceanic conditions, especially during the peak H season (July–September). Specifically, the period 1982–1994 is clearly an active epoch, one with warmer SSTs, lower mean sea level pressures, anomalously stronger low-level cyclonic vorticity, reduced vertical wind shear, and increased precipitable water content across the region (Chu and Clark 1999; Chu 2002). Despite the current quiescent period that began in 1995, enhanced TC activity has occurred in conjunction with El Niño events, which is an obvious concern for the Hawaiian Islands due to the increased probability of TCs developing and impacting the islands (Chu and Wang 1997; Chu and Wang 1998). With the development of an El Niño during the boreal summer, the 2009 season was clearly a more active one. Of note was the formation of MH Neki (Fig. 4.38) that reached Cat- 3 intensity (peak winds of 105 kt), and was the first MH to develop in the sub-basin since 2006 (also an El Niño year). Therefore, the CNP sub-basin reemerged in 2009, which was the most active season in the region since the influence of the strong El Niño in 1997.

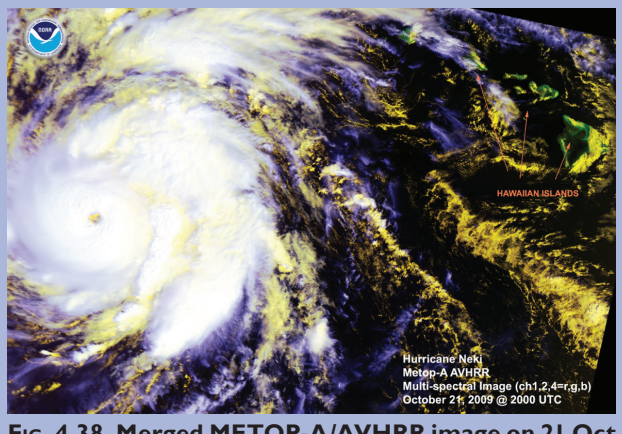

Fig. 4.38. Merged METOP-A/AVHRR image on 21 Oct as MH Neki was located southwest of the Hawaiian archipelago. Maximum sustained winds were about 105 kt (Cat-3) at this image time (2000 UTC), which was during the period of peak intensity for the storm.